Master's thesis

NTNU
Norwegian University of Science and Technology
Faculty of Engineering
Department of Geoscience and Petroleum

Sina Madani

Reservoir Modeling of Smeaheia CO_2 Storage

Master's thesis in Petroleum Engineering
Supervisor: Ashkan Jahanbani Ghahfarokhi
Co-supervisor: Alv-Arne Grimstad
June 2023

NTNU
Norwegian University of
Science and Technology

Sina Madani

Reservoir Modeling of Smeaheia CO_2 Storage

Master's thesis in Petroleum Engineering
Supervisor: Ashkan Jahanbani Ghahfarokhi
Co-supervisor: Alv-Arne Grimstad
June 2023

Norwegian University of Science and Technology
Faculty of Engineering
Department of Geoscience and Petroleum

NTNU
Norwegian University of
Science and Technology

Master's Thesis

Sina Madani

Reservoir Modeling of Smeaheia CO_2 Storage

Master's thesis in Petroleum Engineering

Trondheim, June 2023

Supervisor: Ashkan Jahanbani Ghahfarokhi, NTNU
Co-supervisor: Alv-Arne Grimstad, SINTEF
Norwegian University of Science and Technology
Faculty of Engineering
Department of Geoscience and Petroleum

NTNU

Abstract

CCS, or carbon capture and storage, is a method that can reduce today's carbon emissions. Because the world still heavily relies on fossil fuel energy, this method is essential to achieve the world's net-zero ambitions.

In Norway, a new CCS project in the Smeaheia site has been studied extensively. The project has two significant structures, Alpha and Beta. However, due to the possibility of CO_2 migration to the surface in the Beta area, the Alpha structure is considered the better option. Equinor has developed a reservoir simulation model for Smeaheia, which has been modified in this study for sensitivity analysis of various grid block sizes and using different CO_2-water relative permeability curves.

The significance of relative permeability curves in CO_2 storage projects is emphasized in this study. These curves affect pressure changes, CO_2 movement, and simulation run-time. It is necessary to accurately characterize and calibrate relative permeability values to ensure trustworthy reservoir simulations. Finding a grid size that balances computational efficiency and reservoir representation is essential. The study confirms the feasibility of CO_2 storage in the Alpha structure of the Smeaheia field, which has a capacity of over 80 million tonnes.

Sammendrag

CCS, eller karbonfangst og -lagring, er en metode som kan redusere karbonutslippene i dag. Fordi verden fortsatt er svært avhengig av fossil energi, er denne metoden avgjørende for å nå verdens nullutslippsambisjoner.

I Norge har et nytt CCS-prosjekt i Smeaheia blitt studert grundig. Prosjektet har to viktige strukturer, Alpha og Beta. På grunn av muligheten for at CO_2 kan migrere til overflaten i Beta-området, anses Alpha-strukturen som det beste alternativet. Equinor har utviklet en reservoarsimuleringsmodell for Smeaheia, som i denne studien er modifisert for sensitivitetsanalyse av ulike gridblokkstørrelser og bruk av ulike kurver for relativ permeabilitet mellom CO_2 og vann.

Betydningen av relative permeabilitetskurver i CO_2-lagringsprosjekter understrekes i denne studien. Disse kurvene påvirker trykkendringer, CO_2-bevegelse og simuleringens kjøretid. Det er nødvendig å karakterisere og kalibrere verdiene for relativ permeabilitet nøyaktig for å sikre pålitelige reservoarsimuleringer. Det er viktig å finne en rutenettstørrelse som balanserer beregningseffektivitet og reservoarrepresentasjon. Studien bekrefter at det er mulig å lagre CO_2 i Alpha-strukturen i Smeaheia-feltet, som har en kapasitet på over 80 millioner tonn.

Preface

The thesis, titled "Reservoir Modelling of CO_2 Storage in the Smeaheia Field," meets part of the necessary requirements for the Master's degree in Reservoir Engineering and Petrophysics at the Department of Geoscience and Petroleum at the Norwegian University of Science and Technology (NTNU). The research project was undertaken in partnership with SINTEF Industri AS and the Department of Geoscience and Petroleum (IGP) at NTNU and lasted for six months. The study aimed to model the storage of CO_2 in the Smeaheia Field, a task that required extensive research and analysis. The results of the research provide valuable insights and contribute to the field of reservoir engineering and petrophysics.

Acknowledgement

I am grateful to have had the guidance and support of my supervisor, Ashkan Jahanbani Ghahfarokhi, throughout the completion of this project. Alv-Arne Grimstad provided valuable feedback and insight, for which I am also thankful. My wife deserves recognition for her unwavering support and technical input. Lastly, I extend my gratitude to the Department of Geoscience and Petroleum (IGP) and SINTEF Industri AS for the opportunity to work on this exciting project.

Table of Contents

List of Figures

List of Tables

1. Introduction

This opening chapter presents brief explanation of the motivation behind this master's thesis and its objectives.

1.1. Background

The European Commission has set an ambitious target of reducing human-induced greenhouse gas emissions by 80-95% by 2050, including 500 Gt of CO_2, compared to 1990 levels, as a means to combat climate change (IPCC, 2014) (European_Commission, 2018). Geological sequestration of CO_2 is considered one of the few viable options for effectively mitigating the greenhouse effect by removing greenhouse gas emissions in sufficient volumes. Various groups have conducted aquifer-scale simulations to estimate the storage capacity for CO_2. These simulations typically involve storing CO_2 in a supercritical state, where buoyancy forces drive the injected CO_2 upwards until it reaches a geological seal. However, ensuring the long-term integrity of the seal and the permanence of the stored CO_2 presents challenges that may require costly long-term monitoring.

It is important to understand how injected gas and in-situ fluids displace, especially for deep injection of greenhouse gases in hydrocarbon reservoirs or saline aquifers. Relative permeability and residual-gas saturation are crucial factors to consider in this context. These factors also have significant effects on CO_2 injection in conventional oil reservoirs for enhanced oil recovery (EOR) or in water-alternating-gas (WAG) processes. They impact critical aspects like flow rate, injectivity, gas plume spread, and residual gas trapping. (Kumar, A., Ozah, R., Noh, M., Pope, G.A., Bryant, S., Sepehrnoori, K. and Lake, L.W., 2005)

The Horda Platform offshore Norway has been evaluated extensively and found to be a promising location for the European CCS Cluster. Four potential CO_2 storage sites have been identified, and plans are being made to establish an industrial-scale Horda CO_2 Storage Hub within the next 30 years. It is projected that the amount of CO_2 stored will increase to 810 Mt by 2050 and a significant 1.85 Gt by 2065, indicating a great opportunity for storage in the Horda Platform region (Lothe, A.E., Grimstad, A. and Bergmo, P.E., 2019). These findings provide valuable insights for strategic planning and decision-making in achieving carbon capture and storage goals aligned with the Paris Agreement.

The Smeaheia site, also known as Troll Kystnaer (Lothe, A.E., Grimstad, A. and Bergmo, P.E., 2019) (Lauritsen, 2018) (Statoil, 2016), is located in the Horda Platform and has nine exploration blocks. It is situated about 40 kilometers northwest of the Kollsnes processing plant and 20 kilometers east of the Troll A platform (Troll East). The target aquifers in this area are coastal-shallow marine sandstones from the Viking Group, specifically the Sognefjord and Fensfjord formations (Holgate, 2013) (Furre, 2019). The Horda Platform's east tilting fault block is bounded by two first-order, north-south trending faults, namely the Vette Fault (VF) and the Øygarden Fault (ØGF) (refer to Figure 1).

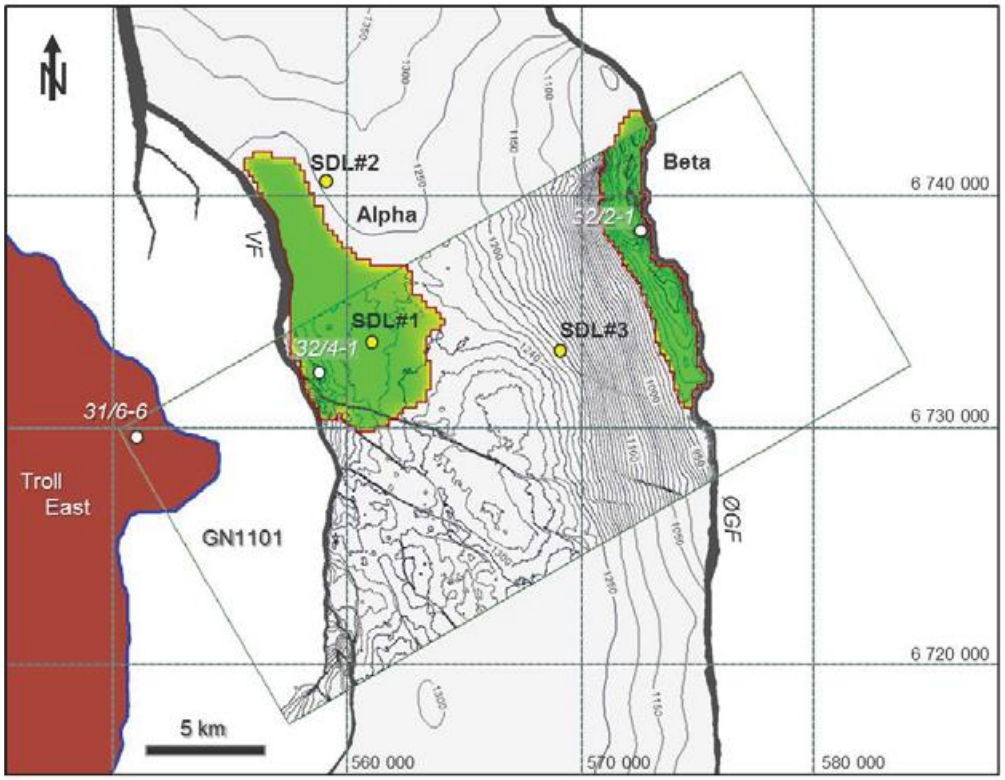

Figure 1 Location of Alpha and Beta structures (VF=Vette Fault, ØGF=Øygarden Fault) (Statoil, 2016)

Two storage prospects, Alpha and Beta (Fig 1) have been identified here. They are formed by footwall and hanging wall three-way structural closures, respectively, and are covered in Upper Jurassic marine claystones from the Draupne Formation (Skurtveit, E., Aker, E., Soldal, M. and Angeli, M. and Wang Z., 2012). The Alpha and Beta prospects were previously drilled in 1996 and 2008, respectively, with the primary goal of exploring the Sognefjord, Fensfjord, and Krossfjord formations for commercial hydrocarbon accumulations (32/4-1 T2 Final Well report, 1997; 32/2-1 Final Well End of well report, 2008). Potential hydrocarbon migration scenarios (Goldsmith, 2000) from neighbouring Troll East were invalidated since neither well indicated hydrocarbon was discovered. The Smeaheia fault block has been suggested as a potential CO_2 storage location due to its sufficient estimated structural storage capacity, excellent reservoir quality, and position relative to the coastline and existing subsea facilities (Elenius, M. and Kaufmann R., 2018) (Statoil, 2016) (Lauritsen, 2018).

In the Smeaheia site, there are two storage possibilities known as Alpha and Beta (as seen in Figure 1). Alpha has a footwall three-way structural closure, while Beta has a hanging wall three-way structural closure. Both storage options are covered by Upper Jurassic marine claystones from the Draupne Formation (Skurtveit, E., Aker, E., Soldal, M. and Angeli, M. and Wang Z., 2012). In 1996 and 2008, drilling activities were carried out to explore commercial hydrocarbon accumulations in the Sognefjord, Fensfjord, and Krossfjord formations. These efforts were unsuccessful in revealing the presence of hydrocarbons, which meant that potential hydrocarbon migration scenarios from the neighboring Troll East field were not valid (Goldsmith, 2000). However, the Smeaheia fault block is now being considered as a potential CO_2 storage location due to its estimated structural storage capacity, good reservoir quality, and proximity to the coastline and existing subsea facilities (Lauritsen, 2018) (Statoil, 2016) (Elenius, M. and Kaufmann R., 2018).

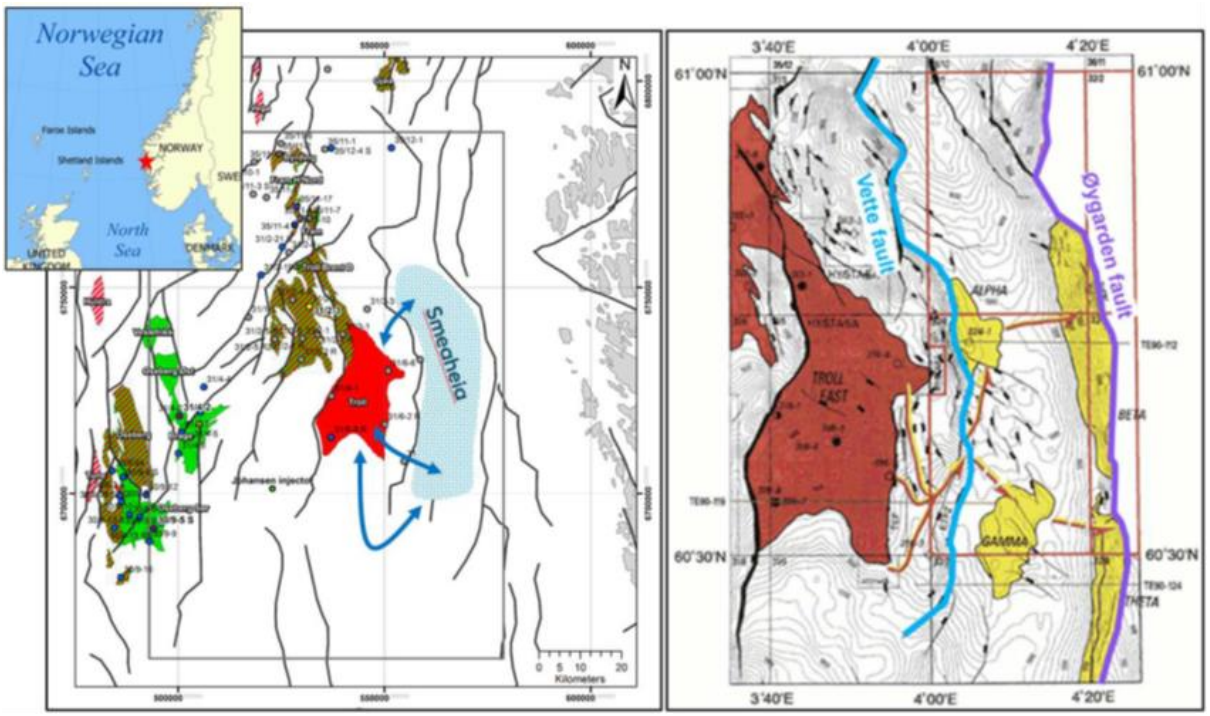

Figure 2 Location of Smeaheia and corresponding faults. (Statoil, 2016)

The assessment of the Smeaheia location has proposed three different development ideas: 1) connecting a subsea well and pipeline to an onshore terminal in the Kollsnes area, 2) injection using a Floating Storage and Injection vessel (FSI), and 3) directly injecting from transport ships. The first two methods involve continuously injecting CO_2, while the last approach uses batch injection (Statoil, 2016). The study area is situated on a fault block that is structurally shallower than the Troll East field, reducing the risk of CO_2 migration and contamination of the Troll reservoir. Consequently, this analysis concentrates on injection in the Alpha zone, as uncertainties remain concerning fault transmissibility and secure storage conditions in the Beta zone. In this study, a sensitivity analysis was conducted to assess the influence of CO_2-water permeability and grid block size on dynamic reservoir simulation performance and CO_2 plume distribution.

Prior to this thesis, the author completed a specialization project that involved analyzing various factors, such as injection rate, perforation depth, well placement, and relative permeability (Madani, 2023). This project was crucial in improving the understanding of the essential elements that affect CO_2 storage simulation in the Smeaheia field. By studying the impact of these factors, the author gained valuable insights into the complexities and dynamics of CO_2 storage simulations, contributing to the overall understanding of the feasibility and effectiveness of CO_2 storage in the Smeaheia field.

A study by Lothe et al. (Lothe, A.E., Bergmo, P., Emmel, B.U. and Eliasson, P., 2018) examined how faults can affect fluid flow and pressure in CO_2 injection and production from the Troll field. Changes in fault properties can significantly impact pressure distribution. By 2072, sealing faults are expected to experience higher pressures (up to 140 bar) compared to intermediate or open faults (around 92-95 bar). Extending faults in two relay zones along the Vette Fault and assuming sealing faults can result in pressures of up to 180 bar. Considering small fluid flow across faults, pressures between 124 and 153 bar are expected by 2072. To accurately forecast and manage CO_2 storage and surrounding oil

and gas fields, it is necessary to address fault uncertainties and complete pre-injection pressure modelling.

An uncertainty analysis has been done by Rahman .et al (Rahmana, M.J., Choib, J.C., Fawada, M. and Mondol, N.H, 2021). This study evaluates the Vette fault's stability for storing CO_2 offshore of Norway, using a stochastic analytical technique, geological knowledge, seismic interpretation, and fault smear possibilities combined. The findings imply that the Vette fault will likely be a barrier during CO_2 injection. The essential criteria are indicated as stresses and fault rock strength. The study emphasizes the need for probabilistic methods for decision-making and fault seal investigation. The reliability of the fault is shown by the fact that the overall chance of failure is within a reasonable range. The results highlight how crucial it is to consider uncertainties while evaluating structures.

1.2. Objectives

The primary objectives of the thesis are as follows:

1. Examine how CO_2 injection is affected by the relative permeability of CO_2-water: The project's primary goal was to investigate how the relative permeability of CO_2-water affected the behaviour of injected CO_2 during reservoir simulation. The project attempted to evaluate how changes in relative permeability affect the flow and distribution of CO_2 inside the reservoir through modification of the relative permeability curves.
2. Assess the sensitivity of reservoir simulation to grid size: The project's goal was to examine how responsive reservoir simulation results were to grid size modifications. In addition, the goal was to determine how changing the static model's grid size, explicitly making it smaller, would affect key simulation parameters like pressure profiles, fluid saturations, and CO_2 plume behaviour.
3. Evaluate the feasibility of CO_2 storage in the Smeaheia field: Based on the outcomes of the reservoir simulation, the project's goal was to evaluate the viability of CO2 storage in the Smeaheia field. The study aimed to assess the reservoir's suitability for long-term CO_2 storage by examining the pressure evolution, CO_2 plume behavior, and storage capacity estimates while considering the updated static model and changed injection settings.
4. Provide insights for CO_2 injection and storage in similar reservoirs: Based on the project's findings, the goal was to offer insightful analysis and suggestions for CO_2 injection and storage in comparable reservoirs. These suggestions covered the relative permeability of CO_2-water, selecting the appropriate grid size for reservoir simulation, and optimizing injection settings for practical storage. In addition, the information was intended to aid in the comprehension and design of CO_2 storage projects in environments with similar reservoirs.

By addressing these objectives, the project's goals were to improve knowledge of CO_2 injection and storage in the Smeaheia field, assess the effects of CO_2-water relative permeability and grid size on simulation results, optimize injection parameters for practical storage, and offer insightful information for CO_2 storage projects in reservoirs with similar geology.

1.3. Outline

The remaining sections of the thesis are presented in a chronological order as follows:

- Chapter 2 - Theory: This section introduces the theories and principles applied in the study, including relevant literature studies.
- Chapter 3 - Methodology: The project workflow is presented, outlining the approach taken to achieve the main objectives.
- Chapter 4 – Results and Discussion: The results of reservoir simulation tasks are presented, along with a discussion of their implications and the study's limitations.
- Chapter 5 - Conclusion: This chapter summarizes the main findings based on the results obtained.
- Chapter 6 - Recommendation for Further Research: This chapter provides ideas for further research.

2. Theory

2.1. Carbon Capture and Storage

CO_2 Capture and Storage (CCS) encompasses a collection of techniques employed within industrial operations to extract carbon dioxide (CO_2) and securely sequester it underground, thereby averting its release into the atmosphere. This process consists of three pivotal steps, each necessitating the utilization of specific technologies, as illustrated in Figure 3 ((IEA), n.d.).

The initial step in CCS is the capture phase, wherein CO_2 is separated from gases generated at expansive industrial facilities, including but not limited to steel mills, cement plants, refineries, and power plants that employ coal or natural gas as a fuel source. This separation is accomplished through the application of dedicated technologies capable of isolating CO_2 from the gas mixture.

Following the capture phase, the next step involves the transportation of the separated CO_2. The extracted CO_2 is compressed and conveyed through various means such as pipelines, trucks, ships, or alternative methods, to a designated storage location deemed suitable for geological sequestration. Transportation methods are implemented to ensure the safe and efficient delivery of the CO_2 to the storage site.

Finally, during the storage phase, the CO_2 is injected into deep subsurface rock formations, typically situated at depths exceeding one kilometer. These geological formations serve as the repository for the stored CO_2, facilitating its long-term confinement and minimizing the risk of leakage or reemission into the atmosphere. By securely sequestering CO_2 within these underground reservoirs, the CCS process effectively mitigates its contribution to greenhouse gas emissions and aids in the reduction of anthropogenic climate change impacts.

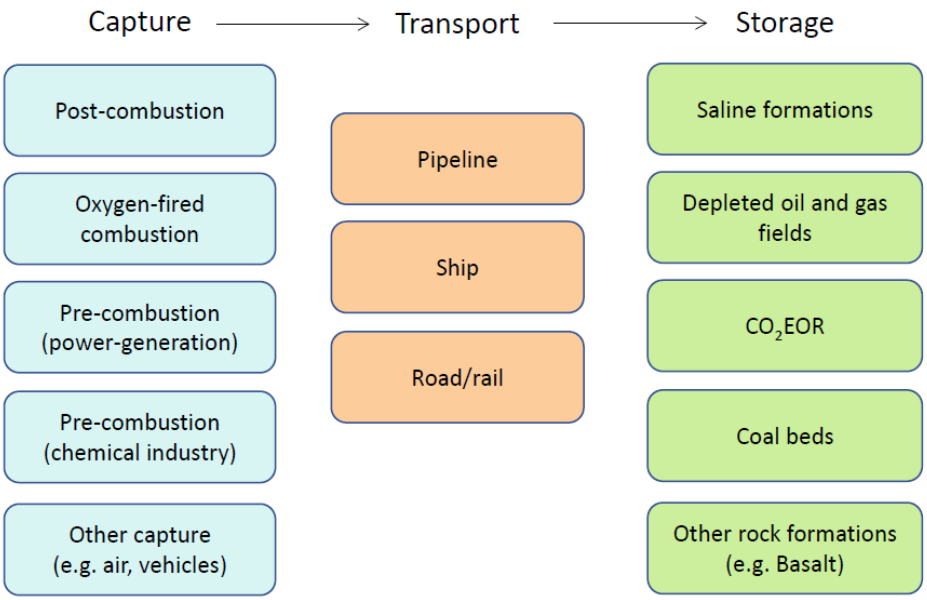

Figure 3 Overview of CCS technologies (Ringrose, 2020)

2.1.1. Capture

Three primary categories or general processes can be utilized to classify CO_2 capture methods or decarbonization technologies. These include post-combustion procedures, precombustion techniques, and denitrogenating methods.

Post combustion procedure

Post-combustion procedures involve the extraction of carbon dioxide from flue gases characterized by low CO_2 content (3-20%) and low pressure (1 bar). The primary objective of separation is to isolate CO_2 from a predominantly nitrogen and oxygen mixture, while considering the presence of flue gas pollutants such as SO_x, NO_x, and particulates. The post-combustion decarbonization process encompasses two main phases: an energy conversion step that generates power and a $_{CO2}$ separation step that yields a concentrated CO_2 stream (Mateus, 2007). Figure 4 provides an overview of the general layout of the post-combustion process.

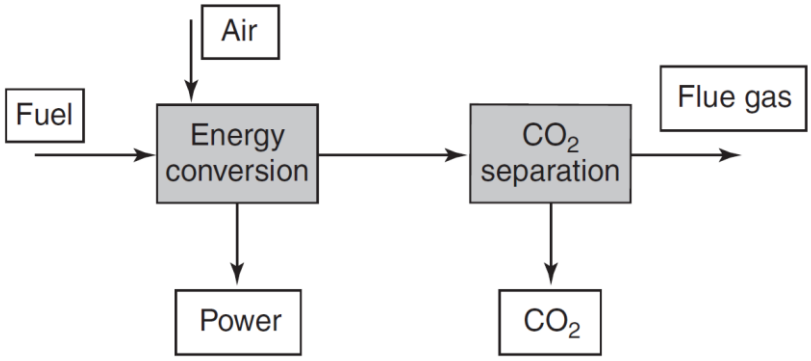

Figure 4 Post combustion decarbonization process (Mateus, 2007)

Precombustion technique

Precombustion techniques, on the other hand, involve the use of a gas mixture with high pressure (15-40 bar) and medium CO_2 content (15-40%) to extract carbon dioxide, or alternatively, carbon can be directly derived from fossil fuels. In addition to CO_2/H_2 separation, the feed gases may also contain CO, H_2S, and other sulfur components. Overall, precombustion decarbonization can facilitate the expedited utilization of H2 as an energy carrier in stationary and mobile applications (Mateus, 2007). It also establishes a connection to an H_2 energy infrastructure based on renewable energy sources. The precombustion decarbonization process comprises three stages: fuel conversion, production of a gas mixture suitable for CO_2 removal, and an energy conversion step that generates power. Figure 5 illustrates the overall flow diagram of the precombustion process.

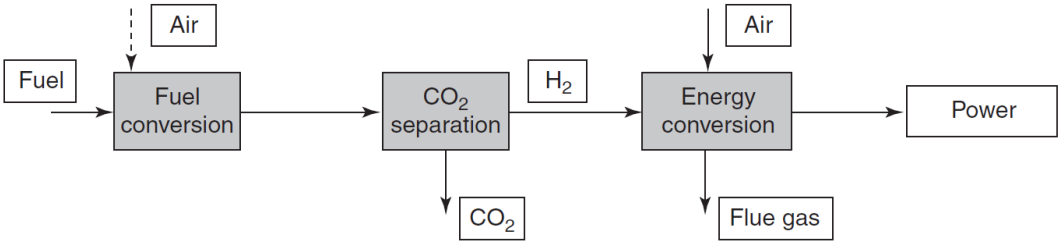

Figure 5 Precombustion decarbonization process (Mateus, 2007)

Oxygen-fired combustion method

Oxygen-fired combustion methods, as another category, involve the separation of nitrogen from the combustion air during the conversion process, keeping it separate from the carbon dioxide produced. The prominent approach in this category is the oxy-fuel process, where O_2 is obtained through an air separation unit, and combustion takes place in an O_2/CO_2 atmosphere achieved through the partial recycling of nitrogen-free flue gas (Mateus, 2007). This distinct process differs from the previous methods in that the separation is focused on producing oxygen from air, eliminating the need for CO_2 separation. An additional advantage is that since the process aims to be flue gas-free, all pollutants are captured in a single step. A high-purity CO_2 stream is subsequently obtained as flue gas. Figure 6 provides an overview of the overall Oxygen-fired combustion process diagram.

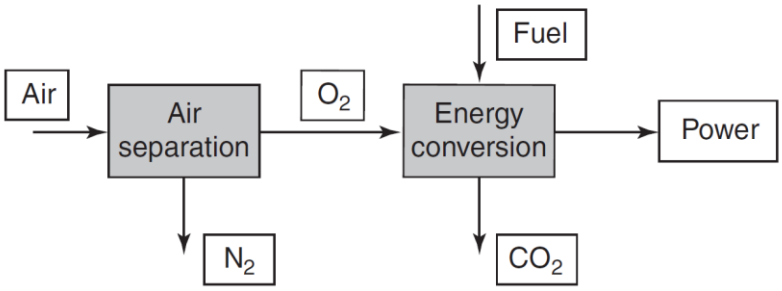

Figure 6 Oxygen-fired combustion process. (Mateus, 2007)

2.1.2. Transport

The transportation of carbon dioxide (CO_2) plays a crucial role in the overall process of a Carbon Capture and Storage (CCS) project, bridging the gap between CO_2 capture and storage phases. This multifaceted operation encompasses several intricate steps, including the compression, liquefaction, and pumping of the captured CO_2 stream, its transportation to an intermediate storage facility, and finally, the delivery to a designated storage site. The CO_2 captured from the source facility is typically transported either in a supercritical phase or in a liquefied state, the latter requiring specific high-pressure and low-temperature conditions as dictated by the CO_2 phase diagram (Figure 7).

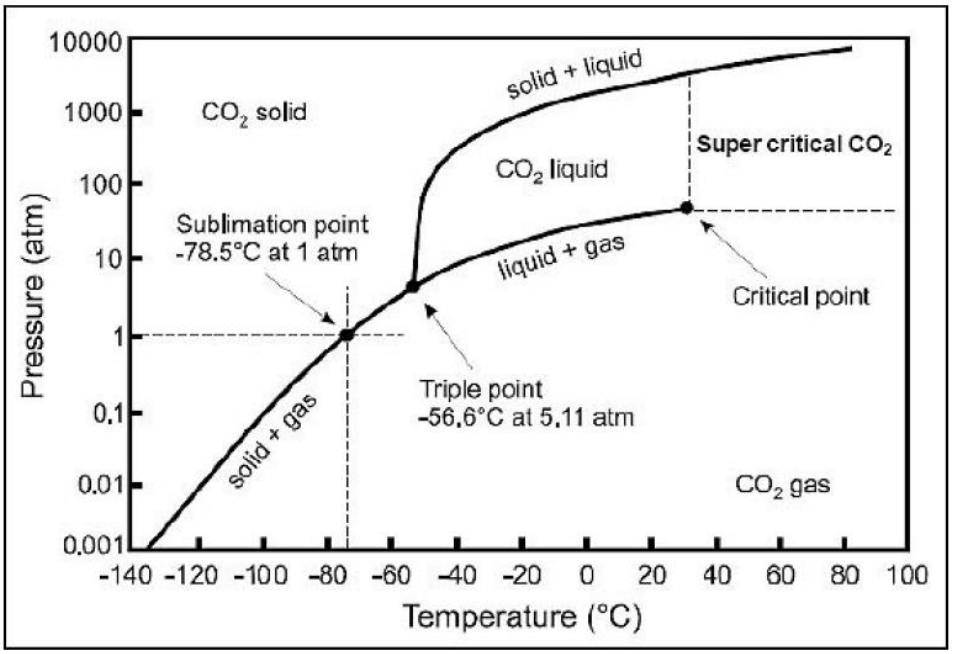

Figure 7 CO_2 phase envelope. (Al-Hinai, K., Al-Bemani, A. and Vakili-Nezhaad, G., 2014)

The challenges associated with CO_2 transport are substantial and demand careful consideration. The transport system must be designed to accommodate the transition of the CO_2 stream across various phase boundaries. Depending on the specific conditions, the CO_2 stream may exist in a gas-phase, liquid-phase, or supercritical phase, necessitating tailored transport conditions. Complicating matters further, impurities such as hydrocarbons, nitrogen, and oxygen may be present in the CO_2 stream, adding complexity to the transport process. Additionally, CO_2 exhibits corrosive properties when in contact with water or oxygen, mandating the use of corrosion-resistant materials (Wildbolz, 2007).

As illustrated in Figure 8, there are several viable options for transporting CO_2-rich gas or liquid streams, with ships, pipelines, railways, and trucks being the most commonly employed methods. The selection of the transportation mode is influenced by various factors, including safety considerations, cost-effectiveness, and efficiency. These factors, in turn, are influenced by the prevailing CO_2 pressure and temperature conditions, geographical considerations, the type of storage site, and the distance between the capture source and the storage complex (Wildbolz, 2007).

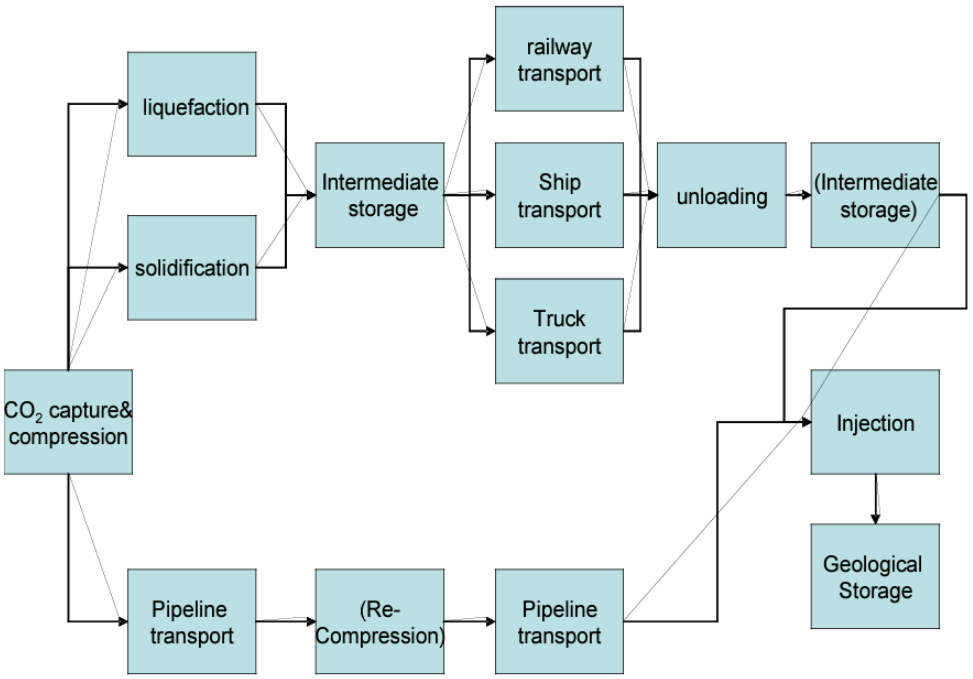

Figure 8 Transport systems for CO_2 (Wildbolz, 2007)

2.1.3. Storage

To effectively mitigate carbon dioxide (CO_2) levels in the atmosphere through storage, the annual capture and storage of a billion metric tonnes of CO_2 are imperative (Rutqvist, 2012). The establishment of secure and long-term storage necessitates careful consideration of several factors. Firstly, a suitable geological formation must be identified, characterized by appropriate pressure and temperature conditions, within which various trapping mechanisms operate over time. Another crucial factor is the distance between the CO_2 source and the storage site, which directly correlates with the chosen transportation method. Generally, closer proximity to the CO_2 source enhances storage opportunities (Cooper, 2009).

Figure 10 presents a typical timeline for the carbon capture and storage process, illustrating the involvement of various functions, each of which may span several years or even a lifetime to complete.

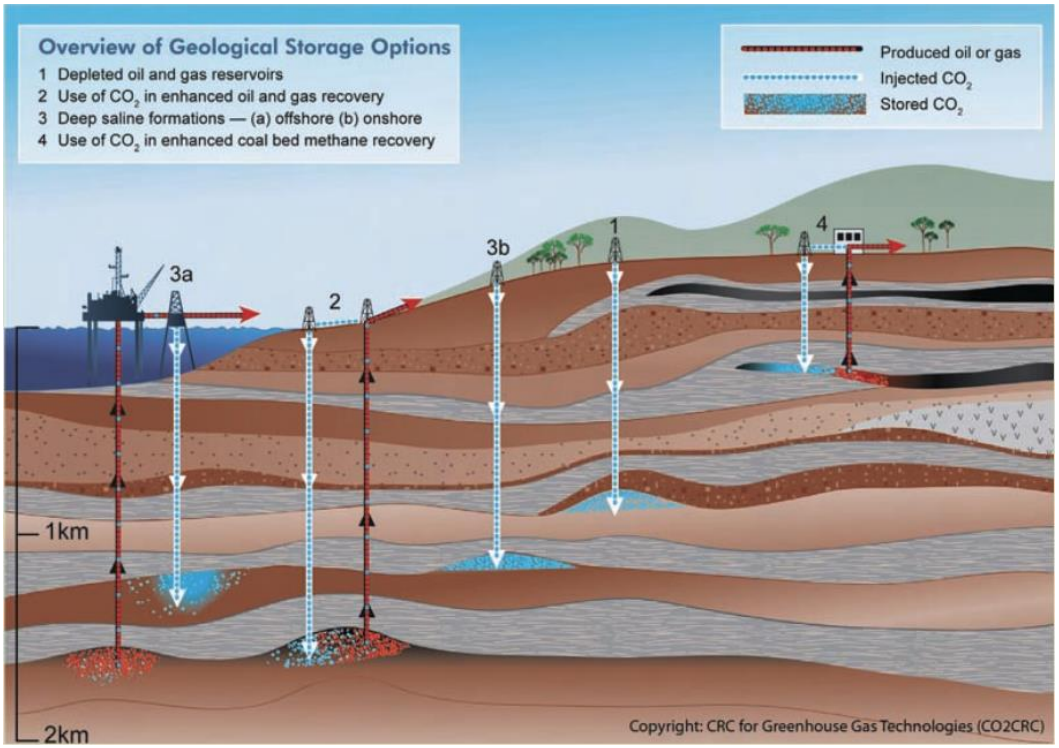

Figure 9 Storage options (Courtesy CO_2CRC)

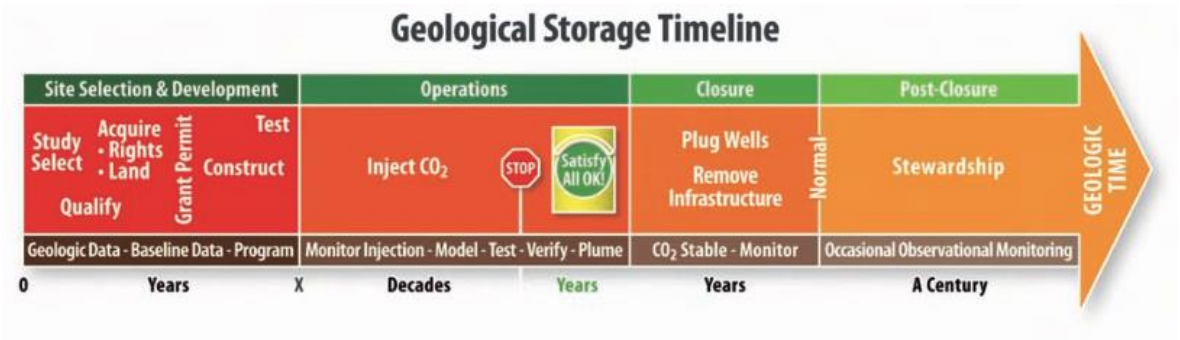

Figure 10 Timeline for CO_2 storage operations (Cooper, 2009)

The depth of storage is crucial in determining whether a storage site is suitable based on temperature and pressure conditions. To ensure that carbon dioxide remains in a supercritical state and efficient caprock containment is achieved, an approximate depth of 800-1000 meters is necessary. Storing carbon dioxide as a supercritical fluid offers better storage capacity and containment capabilities, making it the most efficient and secure option. Figure 11 shows that CO_2 volume decreases as depth increases, emphasizing the importance of storage depth in the overall process.

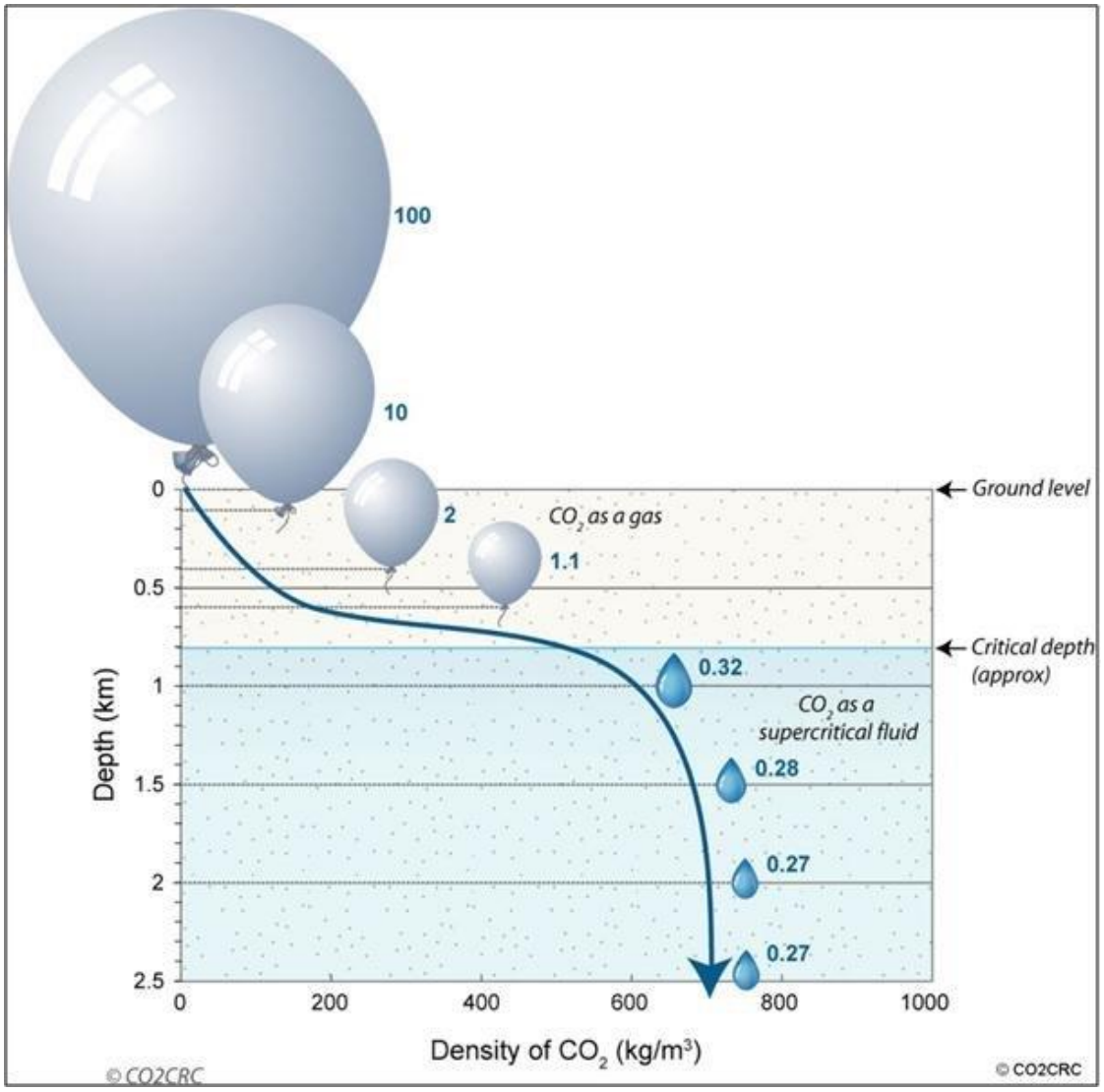

Figure 11 Simplified CO_2 density versus depth diagram.

Various geological structures can serve as potential CO_2 injection storage sites, as depicted in Figure 12. The earliest structured injection of CO_2 into underground geological formations took place in Texas, USA, in 1972, with the primary objective of enhancing oil recovery (Hill, 2013). This project involved injecting 600 million metric tonnes of CO_2, resulting in the production of 1.4 billion barrels of oil, with the produced CO_2 subsequently reinjected.

Once injected, the distribution of CO_2 in geological storage is governed by fluid flow, induced by the pressure gradient caused by injection, natural hydraulic gradients within the storage, buoyancy resulting from density differences between CO_2 and formation fluids, molecular diffusion, dispersion, and fingering in response to heterogeneity and mobility contrasts between CO_2 and formation fluids, dissolution into the formation fluids, mineralization through CO_2 reaction with minerals and organic particles in the formation, pore space trapping, and CO_2 adsorption by organic material. Moreover, for long-term immobilization, CO_2 must undergo physical and chemical trapping mechanisms, as described in Table 1.

TRAPPING MECHANISM	DESCRIPTION
STATIC TRAPPING	Mobile CO_2 is trapped in stratigraphic and structural traps, or in man-made caverns.
STRUCTURAL TRAPPING	Structural traps refer to geological media which precludes the upward and lateral movement of CO_2 induced by crust movement (faults and folds).
STRATIGRAPHIC TRAPPING	Stratigraphic traps refer to geological media which precludes the upward and lateral movement of CO_2 induced by depositional and/or diagenetic processes.
HYDRODYNAMIC TRAPPING	1. The buoyant CO_2 is kept underground by an impermeable caprock. 2. The injected CO_2 is primarily trapped as a gas or supercritical fluid. CO_2 will rise up due to buoyancy effect until it approaches the seals.
CAPILLARY TRAPPING	1. It means the trapping by capillary forces in the pores on the trailing edge of the mobile CO_2 plume (typically). 2. The CO_2 phase is separated into an immobile (trapped) component (or called residual trapping).
RESIDUAL TRAPPING	1. CO2 can be stored as an immobile form in deep saline aquifers due to the density difference between CO2 and brine. CO2 will be left behind as trapped (residual) saturation. 2.CO2 is trapped in the pore space at irreducible gas saturation in which case CO2 is immobile because of the interfacial tension between CO2 and formation water. 3. It means the trapping by capillary forces in the pores on the trailing edge of the mobile CO2 plume (Less commonly). 4. Residual trapping happens when water is imbibed behind the migrating CO2 plume and is caused by gas-water relative permeability hysteresis. 5. Formation of disconnected blobs of CO2 phase is held by capillary forces.
SOLUBILITY TRAPPING (DISSOLUTION TRAPPING)	1. CO_2 dissolves in hydrocarbons or water contained in subsurface formations by diffusion. 2. CO_2 mixes with residual gas. 3. CO_2 dissolves in brine as aqueous species.

MINERAL TRAPPING	1. CO_2 reacts with minerals and organic matters in the geologic formations to become a portion of the solid matrix. 2. CO_2 is trapped by precipitation of carbonate bearing mineral phases, such as calcite, magnesite, siderite, and dawsonite. 3. CO_2 is trapped by the mineralization process of mineral dissolution and precipitation. 4. CO_2 is trapped by precipitation of dissolved carbonate anions and metal cations as solids.

Table 1 Trapping mechanisms. (Ringrose, 2020)

The subsurface storage of CO_2 necessitates careful consideration of various factors. Among these considerations, three key factors play a crucial role in determining the suitability of a formation for CO_2 storage:

Capacity

Capacity refers to the quantity of CO_2 that a specific formation can store, specifically the pore volume available for CO_2 storage. The capacity of a potential storage site is influenced by several variables, including the thickness of the formation, its porosity, the density of CO_2, the area of the storage structure, and the storage efficiency (Cooper, 2009). Additionally, factors such as pressure limitations, barriers, and the size of the storage complex impose significant constraints on capacity (Ringrose, 2020). Pressure limitations, such as the maximum wellhead pressure and fracture pressure, have an impact on the volume of CO_2 that can be injected and stored. Moreover, the size of the formation and the presence of barriers may physically limit the storage capacity.

Estimating the theoretical capacity of CO_2 storage in a porous geological formation's structural or stratigraphic trap involves assessing the available pore volume suitable for storage. This capacity estimation is based on the understanding that the storage potential of a formation depends on the volume of pore spaces within it that can accommodate CO_2. By quantifying the pore volume available for CO_2 storage, it becomes possible to estimate the maximum amount of CO_2 that can be stored within the formation (Ringrose, 2020):

$$V_{CO_2} = V_{trap}\phi(1 - S_{wirr}) \quad (1)$$

(where V_{CO_2} is the theoretical CO_2 storage capacity, V_{trap} is the trap volume, ϕ is the porosity and S_{wirr} is the irreducible water saturation.

The preferred metric for quantifying the amount of CO_2 stored is typically in mass units. Therefore, the CO_2 storage capacity is determined by multiplying the estimated pore volume, denoted as V_b, by the in-situ density of CO_2, represented by ρ_{CO2}. Another factor that influences the theoretical CO_2 storage capacity is the presence of non-sand fractions, expressed as the net-to-gross ratio (NTG). The theoretical estimation does not account for the impact of fluid dynamics, as it assumes that CO_2 storage is solely based on the fraction of pore space filled. To incorporate this effect, a storage efficiency factor (ε) is introduced

(Bachu, 2015). The final expression for the theoretical CO_2 storage capacity, considering all these factors, and measured in mass units, is given by Equation (2):

$$M_{CO_2} = V_b \phi (NTG) \rho_{CO_2} \varepsilon \, (1 - S_{wirr}) \quad (2)$$

The estimated theoretical CO_2 storage capacity, denoted as M_{CO2}, is expressed in mass units. Determining the storage efficiency factor (ε) can be challenging, as it is highly site-specific. In practice, ε typically falls within the range of 0.005 to 0.06, corresponding to less than 6% of the total pore volume (Ringrose, 2020). However, obtaining a more accurate estimation of ε involves employing dynamic flow simulation models and detailed 3D geological reservoir models, which offer improved precision and reliability in the estimation process.

Injectivity

Once the required storage capacity for a carbon dioxide (CO_2) storage project has been estimated, careful attention must be given to the design and management of injection wells and transportation infrastructure. Figure 12 provides an overview of the main engineering aspects of the transport and storage system, with a particular focus on pressure management. Several factors need to be considered in this regard, including reservoir depth, water depth, well design, site performance (plume behavior), reservoir properties, overburden and seal characteristics, and regional aquifer effects.

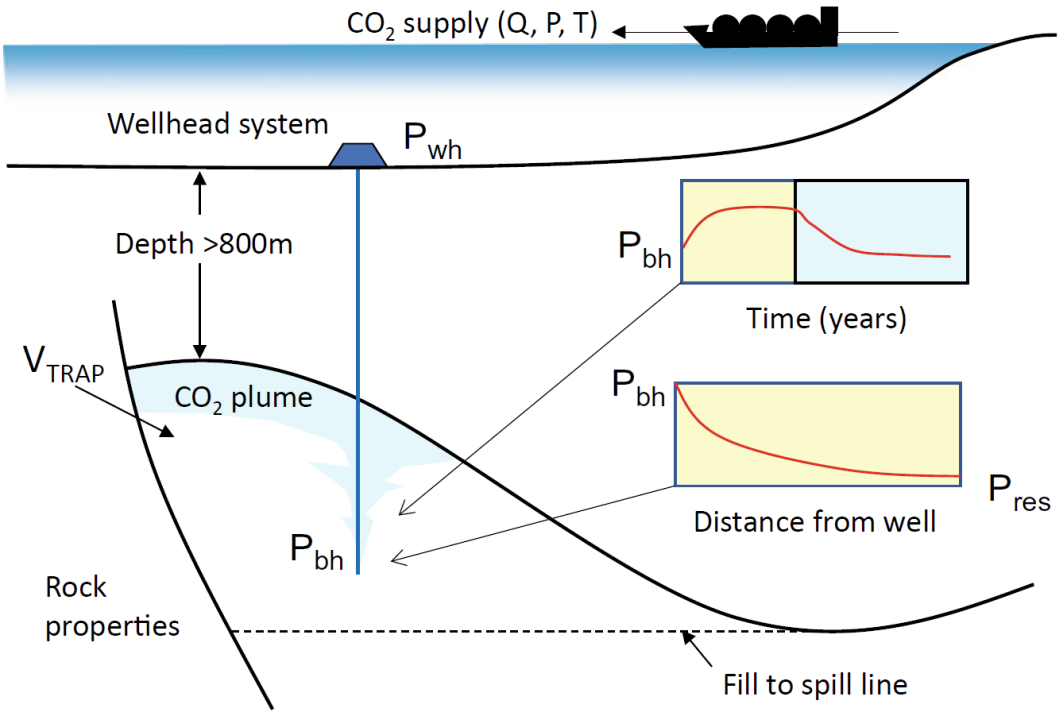

Figure 12 Summary of issues for injection pressure management—based on an offshore setting. (Ringrose, 2020)

Assessing the injectivity of CO_2 injection wells is crucial during site evaluation, alongside considerations of storage capacity and containment. The expected injectivity of a well depends on three major factors: (a) well design, (b) well placement strategy, including well angle and completion length, and (c) reservoir formation properties, particularly permeability.

Ideally, CO_2 storage sites should possess a highly permeable zone near the wellbore, facilitating rapid CO_2 ingress into the pores. However, excessively high permeability formations may have drawbacks (Cooper, 2009). The presence of high-permeability pathways can lead to CO_2 migration, reducing storage efficiency and rendering the formation unsuitable for storage. Additionally, the injected CO_2 may interact with the surrounding rocks and fluids, affecting permeability by either increasing or decreasing it.

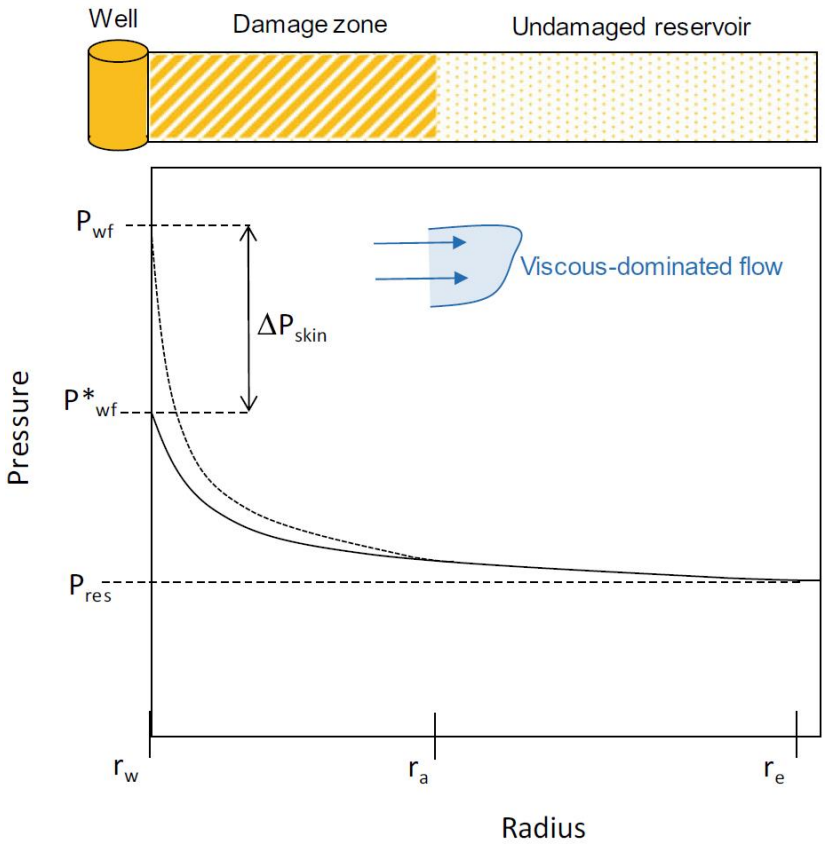

Figure 13 Illustration of effect of near-well damages zone on pressure gradients around an injection. (Ringrose, 2020)

To illustrate injectivity issues, data from the initial years of CO_2 injection at the Sleipner project can be examined. Despite the overall success of the project, the early stages encountered some technical challenges related to injection stability (Hansen, 2005) (Ringrose, 2020). Sand influx into the well resulted in lower-than-anticipated injection rates when using a 100 m perforation interval in a horizontal well at a depth of 1014 m, starting in September 1996. Subsequent installation of sand screens in December 1996 slightly improved injection rates, but significant enhancements in injectivity were achieved only after reperforation of the injection interval in August 1997, along with the implementation of a gravel pack and sand screens over a 38 m horizontal section interval.

These early-stage injectivity problems at Sleipner exemplify a common issue known as the 'skin' effect, which pertains to near-wellbore resistance to injection. This damage to the natural reservoir formation leads to decreased permeability. Near-wellbore damage can result from factors such as invasion of mud filtrates into the formation, local collapse of weakly consolidated sandstone, and migration of fine particles into the pore space.

Figure 12 illustrates the impact of near-wellbore damage on pressure drop, with the dotted line representing the additional pressure drop caused by wellbore damage and the solid line indicating the expected pressure drop in the absence of damage effects. The horizontal axis ranges between the wellbore radius, r_w, and the effective radius of the reservoir, re, with the damage zone radius, r_d, in between. Typically, the flowing pressure at the bottom of the well, P_{wh}, is higher than the anticipated well pressure, P^*_{wh}, as observed in the early stages of Sleipner.

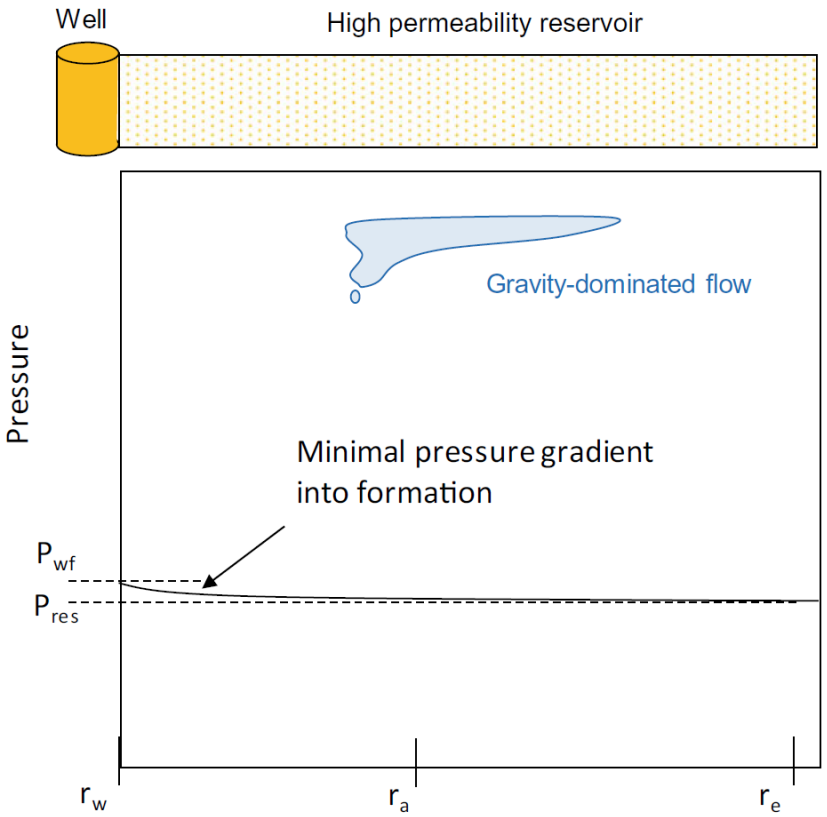

Figure 14 Illustration of effect of pressure gradients around an injection well for high permeability. (Ringrose, 2020)

These near-well effects also influence the distribution of CO_2 within the reservoir, as depicted in the insets of Figures 13 and 14. High formation resistance and steep pressure gradients result in a more viscous-dominated flow regime, while low-pressure gradients near the well lead to the dominance of gravity forces, even in close proximity to the well.

Another significant phenomenon affecting injectivity in CO_2 injection wells is salt precipitation. When brine evaporates at the interface with the injected CO_2 stream, salt crystals can precipitate, particularly when the CO_2 stream has low aqueous content (i.e., very dry CO_2). The partial blocking of pore space by salt crystals can decrease injectivity (Miri, 2015). This effect was observed during the early phases of injection at the Snøhvit site (Grude, S., Landrø, M. and Dvorkin, J., 2014) (Pawar, 2015), and it was also noticed at the Ketzin CO_2 injection pilot project. To mitigate this issue, episodic injections of methyl-ethylene-glycol (MEG) solution were employed at Snøhvit (Hansen, 2005). Consequently, most CO_2 injection projects must evaluate the need for a salt precipitation inhibitor solution in their design, considering the geochemical reactions between reservoir fluid and the CO_2 stream.

It should be noted that each injection well exhibits variations in terms of fluid system, reservoir heterogeneities, and formation characteristics. However, by comparing key metrics of example wells, as illustrated in Figure 12, and drawing upon the lessons learned from early projects, it is possible to gain insights into likely behavioral ranges. Well performance is essentially a matter of engineering design, and as CO_2 storage technology continues to advance, there is ongoing development of optimized well designs, resulting in improved forecasts of injection rates and associated uncertainties for current projects.

Containment

Ensuring the prevention of carbon dioxide (CO_2) leakage from storage facilities is of paramount importance, as any migration of CO_2 out of the formation and into shallow groundwater or the atmosphere would render the storage endeavor futile (Rutqvist, 2012). The effectiveness of containment, which refers to the retention of CO_2 within a storage complex, relies on various factors including seal geometry, rock distribution, pressure regimes, and trapping mechanisms (Cooper, 2009).

Secure storage formations are typically located at depths below 800 to 1000 meters, where impermeable or low-permeable seals are prevalent. The permeability of an average caprock typically ranges from 1 nanoDarcy (nD) to 1 milliDarcy (mD), posing significant challenges for the migration of a CO_2 stream (Ringrose, 2020). However, the presence of seal faults and fractures can significantly impact storage containment. Although the existence of such flaws does not necessarily imply a leakage issue, it is crucial to assess the potential for CO_2 migration under the existing conditions by examining fractures or faults (Cooper, 2009).

Legacy Wells have been identified as one of the most significant risk factors for CO_2 leakage in various assessments related to storage (Pawar, 2015). Specifically, artificially penetrated geological sealing units pose a notable risk.

To monitor the propagation of CO_2 within the storage complex, a range of monitoring technologies can be employed, enabling the identification of any undesirable events. Monitoring can be conducted both at the surface and subsurface levels. Downhole monitoring methods encompass seismic surveys, gravimetry surveys, pressure and temperature monitoring, downhole geophones, and saturation logging. Surface monitoring techniques include soil gas analysis, gas/water chemistry analysis, CO_2 soluble tracers, and biological monitoring. Drawing from project experience thus far, it is possible to delineate the potential composition of future CO_2 monitoring portfolios (Figure 15).

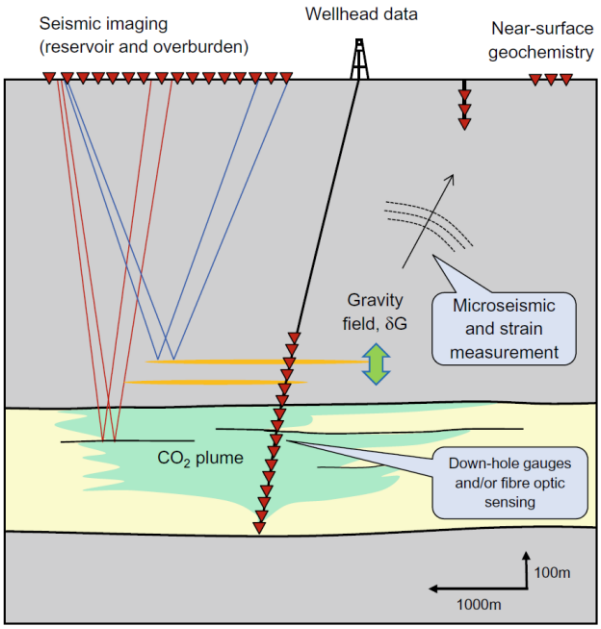

Figure 15 Idealized sketch of a storage site monitoring program.

2.2. Relative Permeability in Porous Media

The capacity of a porous system to conduct a specific fluid when multiple fluids exist within the system is measured by relative permeability, which is a fundamental parameter. Various factors, such as pore geometry, wettability, fluid distribution, and saturation history, influence the flow characteristics. In a uniformly wetted system, the wetting fluid occupies smaller pores and forms a thin film in larger pores, while the nonwetting fluid accumulates in the central regions of larger pores. When comparing different fluids at the same saturation level, the nonwetting fluid generally has a higher relative permeability than the wetting fluid. For example, in an oil-wet system, water exhibits higher relative permeability than in a water-wet system. This behavior is attributed to the preferential movement of the wetting fluid through less permeable smaller pores, while the nonwetting fluid flows more easily through larger pores. At low saturations of the nonwetting phase, the nonwetting fluid forms discontinuous globules within larger pores, obstructing pore throats and reducing the relative permeability of the wetting phase. Conversely, the nonwetting-phase relative permeability remains high as the nonwetting fluid primarily travels through the central regions of larger pores. When the saturation of the wetting phase is low, the effective permeability of the nonwetting phase often approaches the absolute permeability, indicating that the wetting phase has minimal influence on the flow of the nonwetting phase (Doughty, C. and Pruess, K., 2004).

This study used Corey correlations to create gas-oil relative permeability curves. The black-oil model was utilized, with CO2 as the gas and brine as the oil. Petrel software employed the equations 3-6 to generate the relative permeability curves.

Gas:
Corey Gas: For values between S_{wmin} and (1-S_{org}):

$$K_{rg} = K_{rg} \times S_{org} \left(\frac{1 - S_w - S_{gcr}}{1 - S_{wi} - S_{org} - S_{gcr}} \right)^{C_g} \quad (3)$$

where S_{wi} is the initial water saturation.
C_g is the Corey gas exponent.
S_{gcr}: Critical gas saturation.
$K_{rg}@S_{wmin}$: Relative permeability of gas at S_{wmin} (minimum water saturation) value.
$K_{rg}@S_{org}$: Relative permeability of gas at the residual oil saturation value.

Oil:
Corey O/W: For values between S_{wmin} and $(1-S_{orw})$:

$$K_{ro} = K_{ro} \times S_{wmin} \left(\frac{S_{wmax} - S_w - S_{orw}}{S_{wmax} - S_{wi} - S_{orw}}\right)^{C_o} \quad (4)$$

where S_{wi} is the initial water saturation and C_o is the Corey oil exponent.

S_{orw}: Residual oil saturation to water. Note that $(1-S_{orw}) > S_{wcr}$

S_{org}: Residual oil saturation to gas. Note that $(1-S_{org}) > S_{wcr}$

Corey O/G: For values between S_{wmin} and $(1-S_{org})$:

$$K_{ro} = K_{ro} \times S_{gmin} \left(\frac{S_w - S_{wi} - S_{org}}{1 - S_{wi} - S_{org}}\right)^{C_o} \quad (5)$$

where S_{wi} is the initial water saturation
C_o is the Corey oil exponent.
$K_{ro}@S_{omax}$: Relative permeability of oil at the maximum value of oil saturation.

Water:
Corey Water: For values between S_{wcr} and $(1-S_{orw})$:

$$K_{rw} = K_{rw} \times S_{orw} \left(\frac{S_w - S_{wcr}}{S_{wmax} - S_{wcr} - S_{orw}}\right)^{C_w} \quad (6)$$

where C_w is the Corey water exponent
$K_{rw}@S_{orw}$: Relative permeability of water at the residual oil saturation value
$K_{rw}@S=1$: Relative permeability of water at a saturation value of unity
S_{wmin}: Minimum water saturation
S_{wcr}: Critical water saturation. This must be greater than or equal to S_{wmin} (minimum water saturation)

These relative permeability correlations provide valuable tools for characterizing fluid flow behavior in porous media and are selected based on the specific reservoir conditions and wettability characteristics.

Numerous simulation studies have emphasized the importance of multiphase flow properties such as relative permeability and residual CO_2 trapping in CO_2/water systems for characterizing the migration and containment of CO_2 plumes. The final distribution of CO_2 in subsurface formations is highly sensitive to the characteristics of the relative permeability curves. (Doughty, C. and Pruess, K., 2004) (Flett, M., Gurton, R. and Taggart, I., 2004) (Kopp, 2009)

Wegener and Harpole (Wegener, D.C. and Harpole, K.J., 2010) and Burton et al. (Burton, M., Kumar, N. and Bryant S.L., 2009) have highlighted the impact of uncertainties in the relative permeability function on estimates of injectivity and the number of wells required to achieve specific injection objectives.

2.3. Gridding in reservoir simulation

When simulating the flow of fluid in an oil reservoir, gridding is used to create a discrete system that can solve fluid-flow equations. The geological model of an oil reservoir is made up of layers, with faults causing displacement of the strata. It is often not feasible to include all layers in the simulation, so upscaling of rock properties is done. However, even after upscaling, there is still geological heterogeneity within the simulation grid scale.

When choosing a grid for reservoir simulation, two factors must be considered: accurately matching the geological description of the reservoir and discretizing the flow equations. In a classical finite-difference approach, point values of pressures and saturations are used as solution variables, and the differential operators in the fluid-flow equations can be expressed as difference expressions of these point values up to a certain order. However, an integral finite-difference or finite-volume method can also be used, where the fluid-flow equations are integrated over a set of cell volumes. This results in a system of equations where the mass conservation conditions for the fluid in the simulation cell volumes are linked to the flows through the interfaces between those cell volumes. Rock properties, such as porosity, are assumed to be constant within each cell or control volume. This discretization scheme is conservative, ensuring that each outflow from one cell becomes an inflow to another, and facilitates the straightforward determination of fluid in place (Batycky, R.P and Thiele, M.R., 2007).

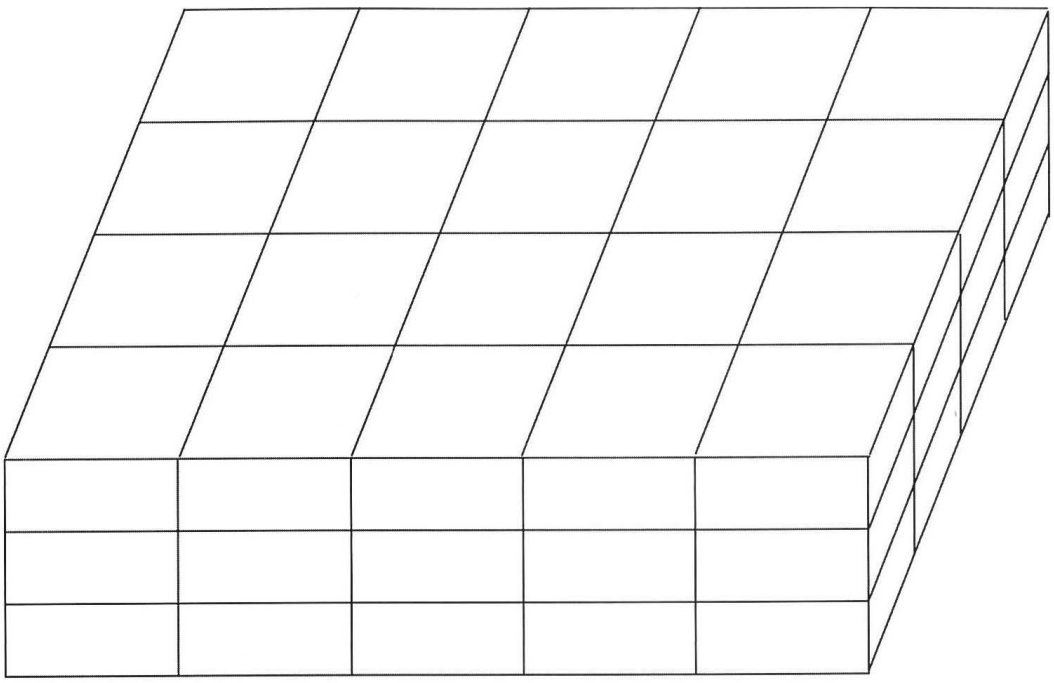

Figure 16 Regular Cartesian grids.

A regular Cartesian grid is a basic three-dimensional grid system that assigns cells unique (i, j, k) index values. Each cell is given a permeability or porosity value, and the transmissibility value is obtained as a harmonic average. Regular grids are typically defined in Cartesian coordinates, but they can also use an (r, ϕ, z) radial system, which is useful for near-well studies that involve radial inflow. These grids yield seven-point schemes in a 30 system, where the flow equations for a cell involve solution values for the cell itself and its six neighboring cells. The grid doesn't have to represent active solution variables in the simulation, and some cells can be inactive, representing volumes of the reservoir with zero porosity. Prior to the memory and computation-intensive flow solution stage, these inactive cells are typically removed from the reservoir simulation solution arrays, allowing for the representation of reservoirs with irregular boundaries within extended simulation grids (Batycky, R.P and Thiele, M.R., 2007).

Rock strata horizons are often not flat, but can be inclined, curved, or faulted. This makes it difficult for a regular grid that is orthogonal in all three dimensions to assign accurate properties to each cell volume in the layer-cake structure (Figure 17). While it is possible to use this type of grid, it often results in property value misalignment. However, with advances in computational power, rasterized grids can now achieve a sufficient level of refinement to create a representative model.

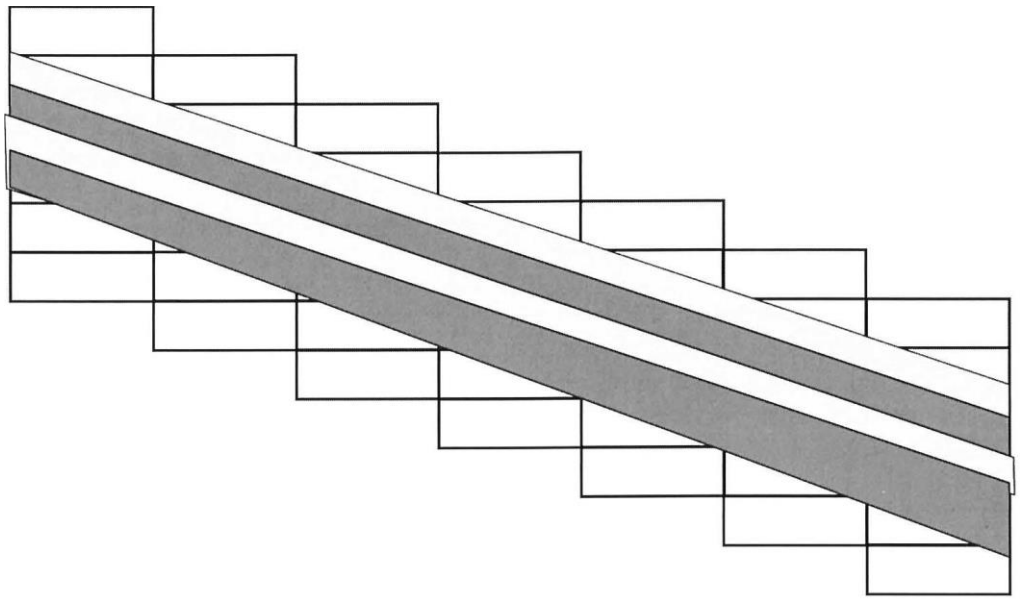

Figure 17 Orthogonal grid used to represent dip.

Dip-Normal Geometry is a modified version of a regular grid that rotates to align the cell layers with the bedding planes. This type of grid is only useful for reservoirs with a constant angle of dip. However, as geological descriptions have advanced, it's clear that fewer reservoirs follow this straightforward pattern. As a result, a more adaptable grid representation is necessary.

The Block-Center Geometry model is a method for calculating the transmissibility between blocks. It uses linear interpolation of the center values of cells to account for variable dip. However, it can be difficult to represent graphically in a consistent way. The model determines pore volumes by using a series of flat regular cells with varying depths. Transmissibilities are then computed using interpolated values. The model's areal grid is rectangular (Batycky, R.P and Thiele, M.R., 2007).

3. Methodology

3.1. Data Availability

The area of interest is located east of the Troll field, between the Vette and Øygarden faults. This region is partially covered by two 3D seismic datasets and multiple sets of 2D seismic lines, as shown in Figure 18. The western structural high, close to well 32/4-1, is associated with Prospect Alpha, while the eastern structural high, near well 32/2-1, is related to Prospect Beta. Gassnova granted Statoil a Petrel project, which entailed interpreting the seismic 3D dataset GN1101, along with velocity and geomodels. The primary focus of the project was on interpreting the seismic data and interpretations for GN1101, since there were no live traces in the area of interest. The TNE01 3D survey was not utilized for interpretation in this case.

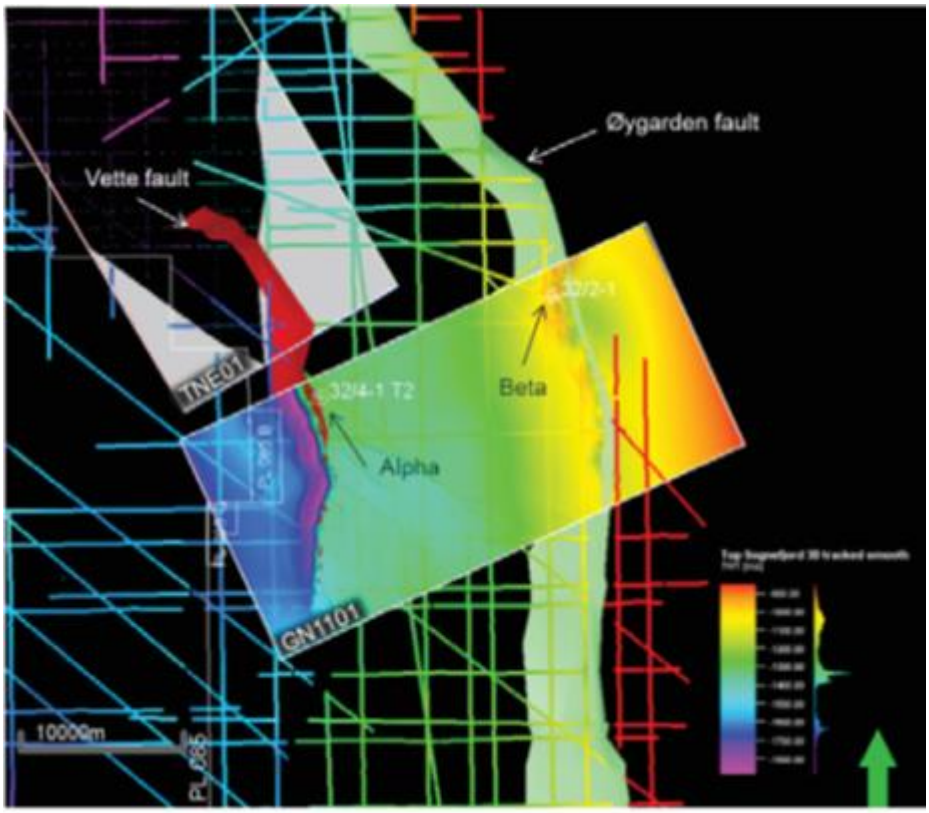

Figure 18 Here is a summary of the seismic datasets utilized in the Smeaheia assessment, including both 3D and 2D formats. The Top Sognefjord TWT surface is outlined in the labeled dataset of GN1101. Unfortunately, the TNE01 dataset had missing live traces in the the grey area. Geological correlation and seismic well ties were conducted with the aid of wells 32/4-1 T2 and 32/2-1. (Statoil, 2016)

Well name	date	Status	TD depth	Cores
32/4-1 T2 (Alpha)	1996 (Philips Petroleum)	Exploration/ P&A/dry	3185m	U.Jurassic
32/2-1 (Beta)	2008 (Talisman)	Exploration/ P&A/dry	1300	-

Table 2 wells used in this report for well correlation and assessment of reservoir quality.

3.1.1. Regional geology and stratigraphy

On the Horda Platform in the north-eastern region of the Stord Basin, there is a storage area called "Smeaheia". The prospects are located on a rotated fault block with large north-south running throw faults bounding it. The Øygarden Fault Zone is situated to the east, while the Vette fault is to the west, acting as a barrier that separates the prospect area from the Troll field. Located in the north-eastern region of the Stord Basin, specifically on the Horda Platform, lies a storage area that goes by the name "Smeaheia". This area boasts of prospects that are positioned on a rotated fault block featuring large north-south running throw faults that surround it. The prospect area is separated from the Troll field by the Vette fault, which acts as a barrier to the west, while the Øygarden Fault Zone is situated to the east.

3.1.2. Geological setting (regional geology and basin evolution)

The Viking Group, consisting of the Krossfjord, Fensfjord, and Sognefjord formations, is present on the Horda Platform, which is characterized by shallow marine environments. The Draupne Formation, resulting from basin-wide flooding, underlies the Viking Group and is overlain by the Base Cretaceous Unconformity or, in some cases, the Lower Cretaceous Cromer Knoll Group due to erosional processes. The initial stages of the rifting process led to the formation of the Krossfjord Formation, characterized by the progradation of sand-rich deltas. Geological activity on the Horda Platform has been relatively limited, with minimal normal faulting and fault-block rotation occurring. However, during the middle Callovian period, sediment input exceeded subsidence rates in the basin, resulting in the development of the Fensfjord Formation, which eventually covered the Horda Platform. In the late Callovian period, fault-related subsidence overtook sediment supply, causing the inland migration of the Fensfjord Delta. Fault-related activity during this time also led to the formation of footwall islands that served as additional sources of sediment input. Towards the end of the late Callovian period, a marine transgression occurred (Statoil, 2016).

During the rifting event in the Oxfordian-Kimmeridgian period, the Sognefjord Formation was formed as a syn-rift wedge. Increased uplift caused the footwalls of fault-blocks to emerge above sea level, resulting in erosion on their crests. The older sediments of the Sognefjord Formation were subsequently reworked and redeposited (Holgate, 2013).

In the Troll area, the Sognefjord Formation acts as the primary reservoir. It exhibits a thickness ranging from 100 to 170 meters, and the individual target sands within the formation can vary in thickness from 3 to 45 meters, with permeability ranging from 1 to

20 Darcy. These sands are interbedded with finer-grained micaceous units. Both the Sognefjord and Fensfjord formation contain calcite cemented zones, typically a few meters thick, with lateral extents ranging from tens of meters to a few kilometers (Dreyer, T., Whitaker, M., Dexter, J., Flesche, H. and Larsen, E., 2005). Figure 19 provides a visual depiction of the stratigraphy of the Horda Platform.

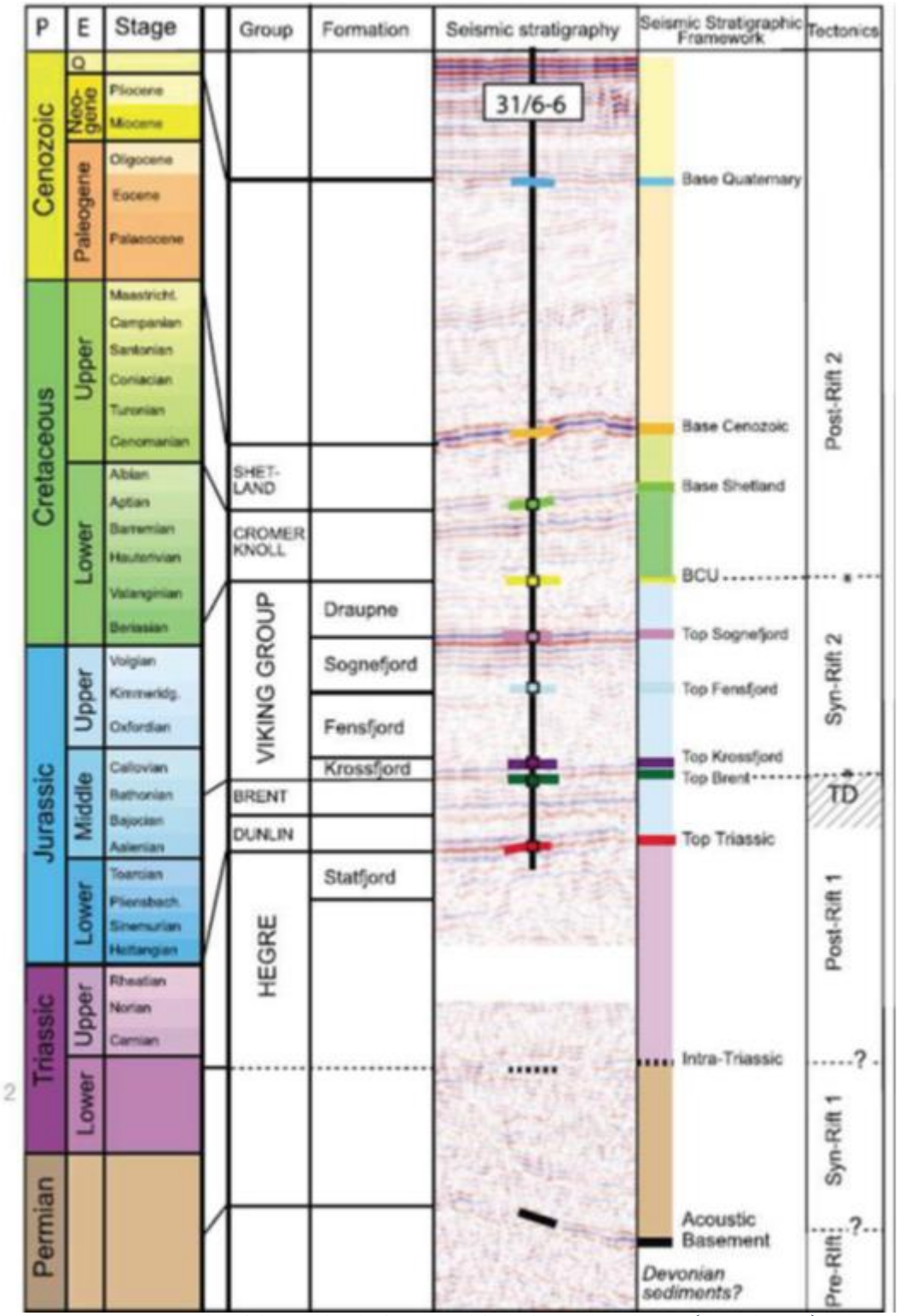

Figure 19 Stratigraphy of the Horda Platform. Modified after Bell et al, 2014 (Statoil, 2016)

3.2. Structural closure capacity estimate

This assessment provides an estimate of the storage capacity for potential prospects. It assumes that the prospects are filled to their maximum capacity and takes into account siltstone intervals based on the estimated net reservoir. However, it's important to note that lateral siltstone baffles, like those observed at Sleipner, can significantly increase trap capacity due to stacked and layered plume dispersion. For a more accurate estimate in such scenarios, detailed dynamic modeling is necessary.
When CO2 is injected into a reservoir, it can displace water and reach the maximum gas-water contact, which is the depth of the spill point. If CO2 is injected below the spill point depth of 1240 m specifically for well Alpha, it can help increase capacity by sweeping additional volumes. This is because the residual CO2 saturation in the reservoir below Alpha's flank will be retained. To estimate capacity that includes the swept residual volumes, we need to perform dynamic reservoir simulation. structural closure capacity estimate (Masssc) can be calculated by using Equation 7:

$$Masssc = BRV_{trap} \times NTG \times \varphi_{res} \times Sat_{gas} \times \rho_{gas} \quad (7)$$

- Apply a constant estimated bulk rock volume (BRV_{trap}) for the mapped structural closure.
- Apply the estimated net-to-gross range (NTG) for the reservoir, assuming a uniform distribution.
- Apply the estimated reservoir porosity range (Phi_{res}), assuming a normal distribution.
- Apply the estimated gas saturation (Sat_{gas}) for the reservoir, assuming a uniform distribution.
- Assume reasonable CO2 density (ρ_{gas}) for given PVT conditions.

	LOW CASE	MID CASE	HIGH CASE
BULK ROCK VOLUME (M^3)	634 000 000	634 000 000	634 000 000
NET (%)	75	85	95
PERMEABILITY (MD)	440	1300	4000
POROSITY (%)	31	35	39
SATURATION (%)	70	80	90
STRUCTURAL CAPACITY (MT)	**82.7**	**98.6**	**117**

Table 3 Structural capacity estimate for Alpha prospect (Statoil, 2016)

3.3. Static Modeling

In this study, the Static model provided by Statoil and accessible through CO_2 Datashare (CO2Datashare, n.d.) was employed. Thorough extraction of pertinent data from Statoil's reports on the Subsurface Evaluation of Smeaheia was conducted to ensure the accuracy of our research.

Geological and petrophysical modeling was carried out utilizing the IRAP RMS software. The most recent interpretation of the Top Sognefjord surface was employed to generate the current model for gridding purposes. In order to create the bottom surface, a duplication of the Top Sognefjord surface was made, and it was subsequently shifted 400 meters deeper due to uncertainties surrounding the Base Krossfjord surface. This adjustment was made based on the understanding that the Krossfjord formation exhibits poor reservoir quality and the tilted nature of the Top Sognefjord surface indicates the presence of the Base Krossfjord. A regular mesh was created with a lateral resolution of 200 x 200 meters, dividing the reservoir depth into 40 layers to achieve a vertical resolution of approximately 4 meters (Statoil, 2016). In this study the mesh resolution has been modified as described in section 3.3.1.

To assess the static characteristics of the Sognefjord, Fensfjord, and Krossfjord formations, log data obtained from exploration wells 32/4-1 T2 and 32/2-1 were analyzed. Petrophysical modeling was performed using the IRAP RMS software. The reservoir was subdivided into three zones, each containing three facies representing sand of good quality, sand of poor quality, and shale, as identified through log observations. Petrophysical modeling was conducted separately for each zone and facies to determine the permeability distribution, while porosity values were derived using correlations with permeability values (Statoil, 2016).

Statoil has developed a grid spanning an area of 20 x 34 kilometers, encompassing both the Alpha and Beta structures. This grid facilitates the examination of potential CO_2 flow from the Alpha structure to the Beta structure through spill points, thereby enabling an exploration of such possibilities.

3.4. Dynamic Modeling

In this section, we will discuss the underlying assumptions employed to model the movement of CO_2 and forecast the storage capacity within the reservoir. The simulations were conducted utilizing the Eclipse Black-Oil Simulator E100, while Petrel 2019 was employed for data visualization and management of diverse injection scenarios. To enhance modeling flexibility for the liquid phase, CO_2 was simulated as a gas and water as oil, allowing for improved control over dissolution rates, which play a critical role in accurately predicting the behavior of CO_2 movement and storage within the reservoir.

To replicate the 40-bar reservoir pressure reduction resulting from production activities in the Troll field (Statoil, 2016), the Statoil model was employed, employing five production wells. However, the precise impact of this depletion on the reservoir pressure at Smeaheia remains uncertain and necessitates further investigation. A comprehensive understanding of the effects of reservoir pressure changes is crucial for accurately assessing CO_2 storage capacity and predicting the long-term behavior of the storage site.

The simulations conducted in this study spanned a 25-year injection period from 2022 to 2047, a production period from 1998 until 2060, with monitoring extended until 2072. This extended monitoring period enables a comprehensive evaluation of the long-term effects of CO_2 storage, encompassing potential migration or leakage concerns.

3.4.1. Grid Size

To analyze the effect of grid size on reservoir simulation results, we conducted a sensitivity analysis using three different grid models with sizes of 200 meters, 150 meters, and 100 meters. Petrel grid functions were used to ensure consistency and accuracy in the grid generation process. To ensure that the fine grids accurately represented the reservoir's static properties, we used petrel upscaling methods with the "Target cell center" sampling method. This method allowed us to convert static properties from the original coarse grid to the finer grids, resulting in a more precise representation of the reservoir's heterogeneity and flow behavior at smaller length scales.

By utilizing these petrel upscaling methods, we maintained the integrity of the simulation results and ensured that the flow behavior on the finer grids was consistent with the reservoir's geological characteristics. The three different grid models, each with a distinct grid size, allowed us to assess the impact of grid size on key performance indicators such as fluid flow rates, pressure distribution, and CO_2 plume behavior.

It's worth noting that the choice of grid size in reservoir simulation requires a trade-off between computational efficiency and accuracy. Finer grids provide more detailed representations of the reservoir's heterogeneity and flow behavior, but they also increase computational requirements. Coarser grids offer faster simulations but may sacrifice accuracy in representing the reservoir's intricate features.

This sensitivity analysis of grid size will provide valuable insights into optimizing grid resolution for future reservoir simulations. It will help determine an appropriate balance between computational efficiency and accurate representation of the reservoir's dynamic behavior.

3.4.2. Cut model

To overcome the computational difficulties linked to smaller grids, the model's development and modification followed a strategic approach within the methodology. As mentioned earlier, the model was deliberately trimmed from the southern part in the J direction, with a particular emphasis on the Alpha structure, which was the focus of the study.

Our main focus was on the Alpha structure, so we intentionally trimmed the model from the southern part in the J direction. This resulted in the removal of 795,000 grid blocks from the original coarse grid model with a 200m grid size. This reduction was aimed at improving computational efficiency while still maintaining the essential geological features and flow behavior of the Alpha structure.

In order to accurately depict the observed reservoir pressure trend during simulation time from the original model, some adjustments were made to the southern part of the modified model. This included applying a transmissibility multiplier (in the Y direction) of 0.1 and 0.2 and a pore volume multiplier of 40 for 200m and 100m models and 48 for 150m model. Also, the production rate for two wells on the 100m model has been reduced from 4000 sm3/day to 2000 sm3/day. The purpose of these modifications was to replicate the reservoir pressure conditions and ensure consistency with the original model. (Figure 21)

Grid Size	PV multiplier	Transmissibility multiplier	Well 1 production rate	Well 2 production rate	Well 3 production rate	Well 4 production rate	Well 5 production rate
100m	40	0.2	4000	4000	4000	2000	2000
150m	48	0.1	4000	4000	4000	4000	4000
200m	40	0.1	4000	4000	4000	4000	4000

Table 3 Cut model modifications.

Furthermore, in order to align the production wells with the southern part of the new model resulting from the cut, four production wells were moved north be in the southern of the new model. (Figure 20) This adjustment ensured that the production wells remained positioned within the southern area of the modified models, where the main focus of the study was centered.

By implementing these modifications and adjustments, the methodology ensured that the new models accurately represented the Alpha structure, maintained consistency in reservoir pressure distribution, and aligned the production wells with the appropriate region of interest. These steps were essential for conducting reliable simulations and obtaining meaningful results for the analysis of CO_2 movement and storage within the reservoir.

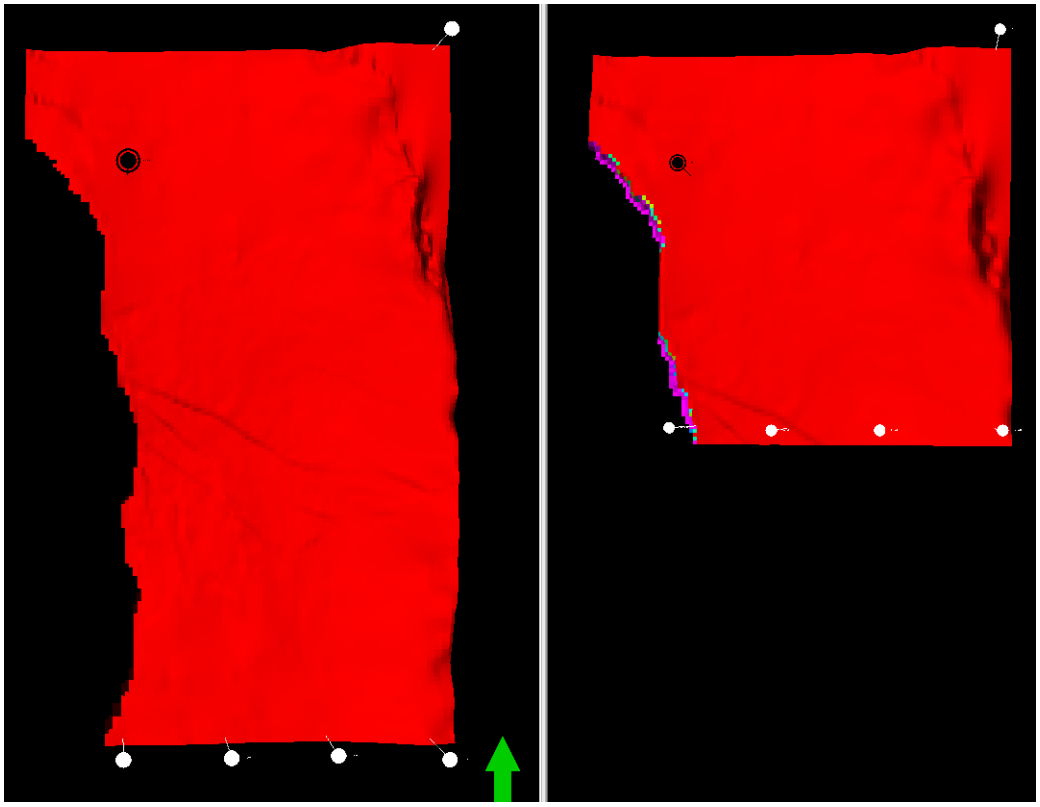

Figure 20 In the left picture, we can observe the initial model, whereas the right picture displays the top view of the modified model. The black dots represent the injection wells, and the white dots symbolize the production wells.

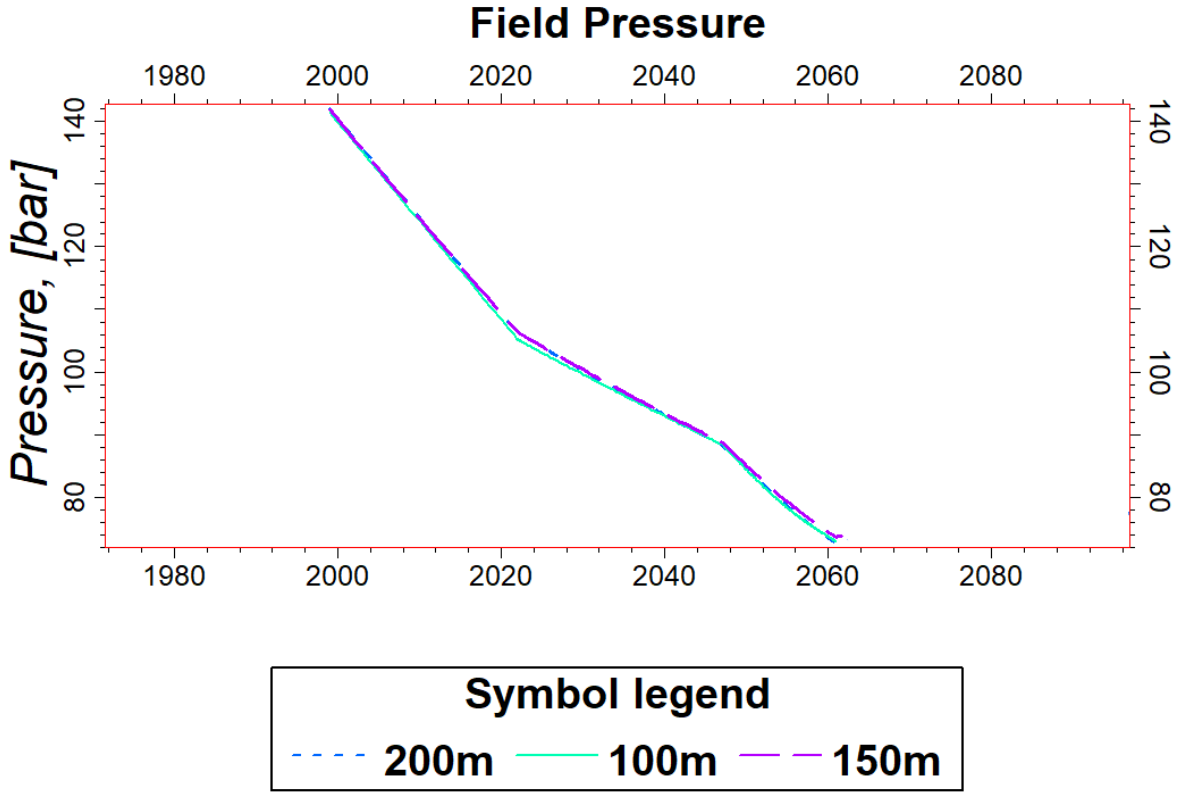

Figure 21 This plot depicts the field pressure profile of the cut model throughout the simulation's injection period for three different grid sizes. It is evident that all three models exhibit the same pressure profile.

3.4.3. Well design

In the current stage, it is recommended to employ a vertical appraisal well design with a comprehensive coring and logging program, which can later be converted into a vertical injector. The determination of the optimal perforation interval(s) for injection was based on previous research findings (Madani, 2023).

The choice between vertical and horizontal orientations of the injection well bears significant implications for the distribution and storage of CO_2 within the reservoir. While vertical injection wells have long been utilized, benefiting from extensive industry expertise, horizontal and multilateral wells have emerged as the preferred options in reservoir development (Li, Z., Fernandes, P. and Zhu, D., 2011).

The length of the wellbore plays a critical role in optimizing CO_2 injection strategies. A horizontal wellbore, being considerably longer than a vertical one, exposes a larger portion of the wellbore to the formation. This elongated configuration results in a larger perforation area, thereby improving the injection or production rate (Anon., n.d.). Additionally, a larger perforated area contributes to a reduced pressure drop, promoting a more balanced inflow and outflow of fluid, thereby enhancing injection or production flow dynamics. Moreover, a horizontal well configuration leads to lower fluid velocities near the wellbore, furnishing valuable insights into the lateral geology of the reservoir, and minimizing the occurrence of water and gas coning (Anon., n.d.).
Considering these advantageous characteristics, a horizontal injection well has been selected for all simulations conducted within this research. The specific injection well, denoted as Alpha N, is visually depicted in Figure 22, encompassing a horizontal segment spanning ten grid blocks, equivalent to approximately 1900 meters.

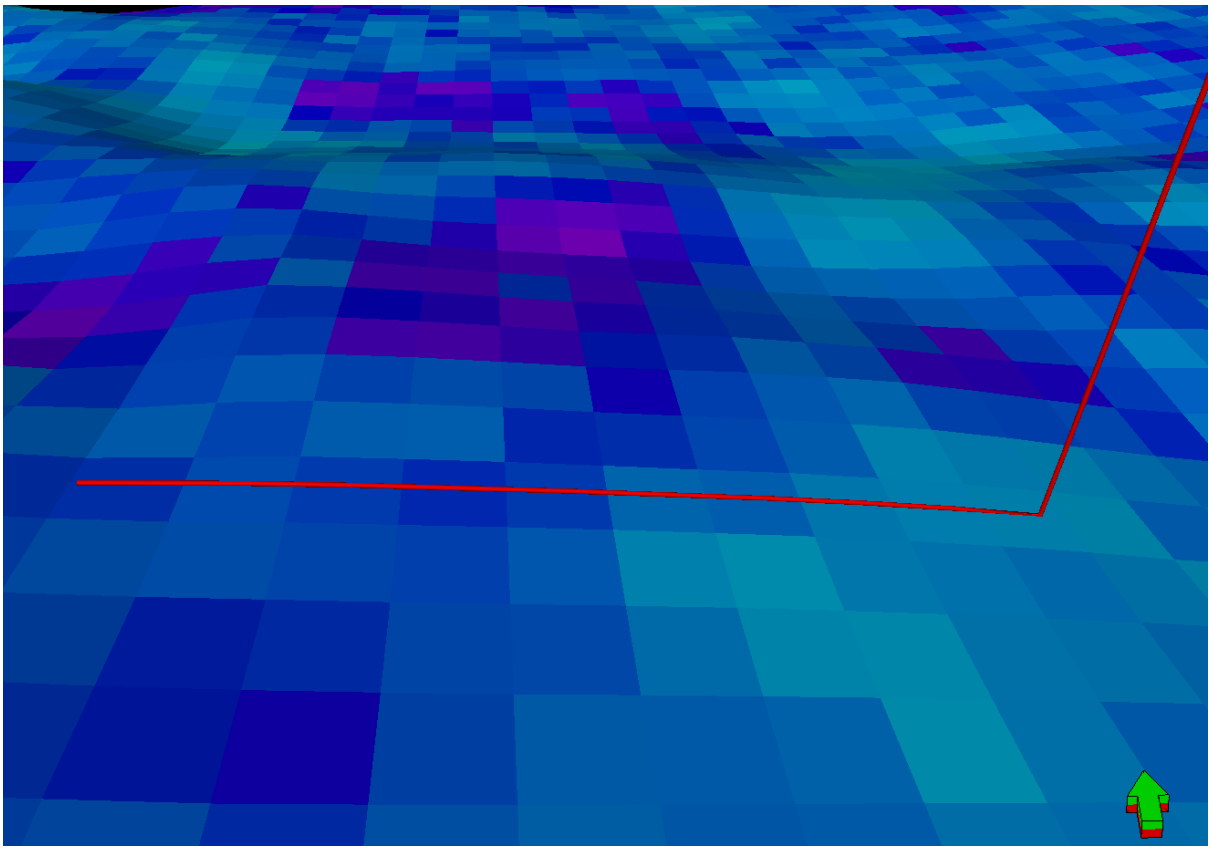

Figure 22 Horizontal injection well in the Alpha structure.

3.4.4. PVT and flow property modelling

In this study, dynamic simulations were conducted utilizing Eclipse black-oil models, as previously reported in the Statoil report. These models represent CO_2 as a gas by incorporating its properties into the gas phase. Brine, on the other hand, is modeled using oil. The utilization of Eclipse models offers enhanced modeling flexibility for the oil phase, thereby providing improved modeling possibilities.

The PVT (Pressure-Volume-Temperature) data for the Smeaheia model was derived from the modeling work conducted by Gassnova. This data is based on reservoir temperatures of approximately 37 °C, which approximately corresponds to the reservoir temperatures of the Alpha and Beta structures, namely 45 °C and 35 °C, respectively. The initial conditions of the simulation are summarized in Table 6.

PROPERTY	INITIAL VALUE
DATUM DEPTH	-800 m
PRESSURE	81 bar
OIL DENSITY (AQUIFER)	1026.0302 kg/m^3
GAS DENSITY	1.8719 kg/m^3
ROCK COMPRESSOBILITY @ P=10 BAR	4E-05 bar^{-1}

Table 4 Initial reservoir conditions

For the current simulation scenarios, the dissolution of CO_2 in brine has been disregarded, resulting in a conservative approach to estimating the extent of CO_2 plume movement. Statoil utilized linear relative permeability data obtained from Gassnova in their simulation. However, in this study, different relative permeability curves have been employed to investigate the influence of relative permeability on plume movement and storage capacity. Specifically, three distinct oil-gas relative permeability curves for sand were generated using the Corey default model in Petrel. It is worth noting that these curves share the same endpoints as the linear permeability curve (Except S_{org}. changed to separate curves in gas saturations between 0.8 and 0.9), as depicted in Figure 23. The parameters employed for generating these curves are presented in Table 7.

Rel-perm model	S_{gcr}	Corey gas exponent	$K_{rg}@S_{wmin}$	$K_{rg}@S_{org}$	S_{org}	Corey O/G	$K_{ro}@S_{omax}$	S_{wmin}
Linear	0.05	-	0.95	0.65	0.1	-	0.8	0.1
Relperm1	0.05	1.5	0.95	0.65	0.15	1.5	0.8	0.1
Relperm2	0.05	2	0.95	0.65	0.1	2	0.8	0.1
Relperm3	0.05	3	0.95	0.65	0.08	3	0.8	0.1

Table 5 Input parameters for generating Corey relative permeability curves using petrel rock physics function.

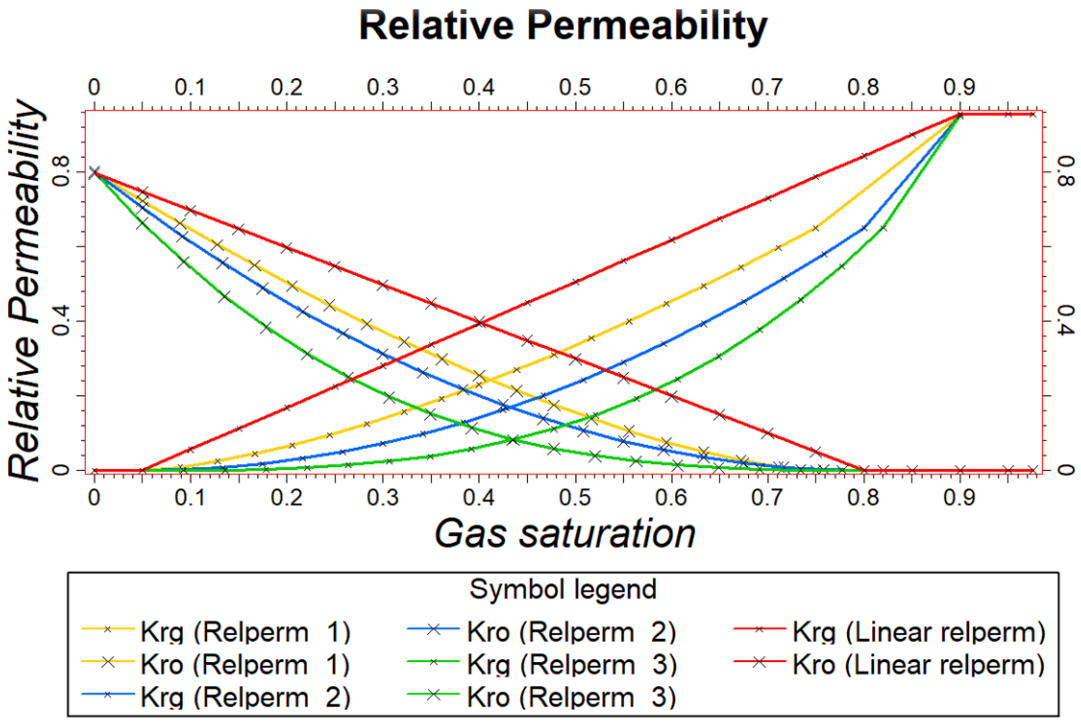

Figure 23 Corey relative permeability curves and the linear relative permeability curve (red color).

4. Results and Discussions

This section presents the results and discussion of the master's thesis, focusing on the movement of the CO_2 plume in the Alpha structure of the Smeaheia storage area. By injecting CO_2 into the formation, the carbon dioxide content increases, forming a plume. The analysis explores the impact of grid size and relative permeability on the movement of the CO_2 plume, considering 12 models with varying grid sizes and relative permeability curves. The objectives of the thesis include examining the behaviour of CO_2 injection influenced by relative permeability, assessing the sensitivity of reservoir simulation to grid size, optimizing CO_2 injection parameters for efficient storage, evaluating the feasibility of CO_2 storage in the Smeaheia field, and providing insights for CO_2 injection and storage in similar reservoirs.

4.1. CO2 Distribution

When CO_2 is injected into the Alpha structure, it flows through the pores and into the formation, causing the carbon dioxide content to rise and form a plume. To ensure stability in the storage site, it's important to determine the optimal volume of CO_2 injection that creates a stable plume. Understanding how CO_2 might flow in the Smeaheia storage area is crucial in determining this. Figures 24-26 illustrate CO_2 movement across the Smeaheia storage site when 9000 tons of CO_2 is injected daily (89.125 MT total) at perforation depth of 1600m (layer 76) for all cases. The results are shown for different grid size and relative permeabilities. The black dots indicate the location of the injection wells.

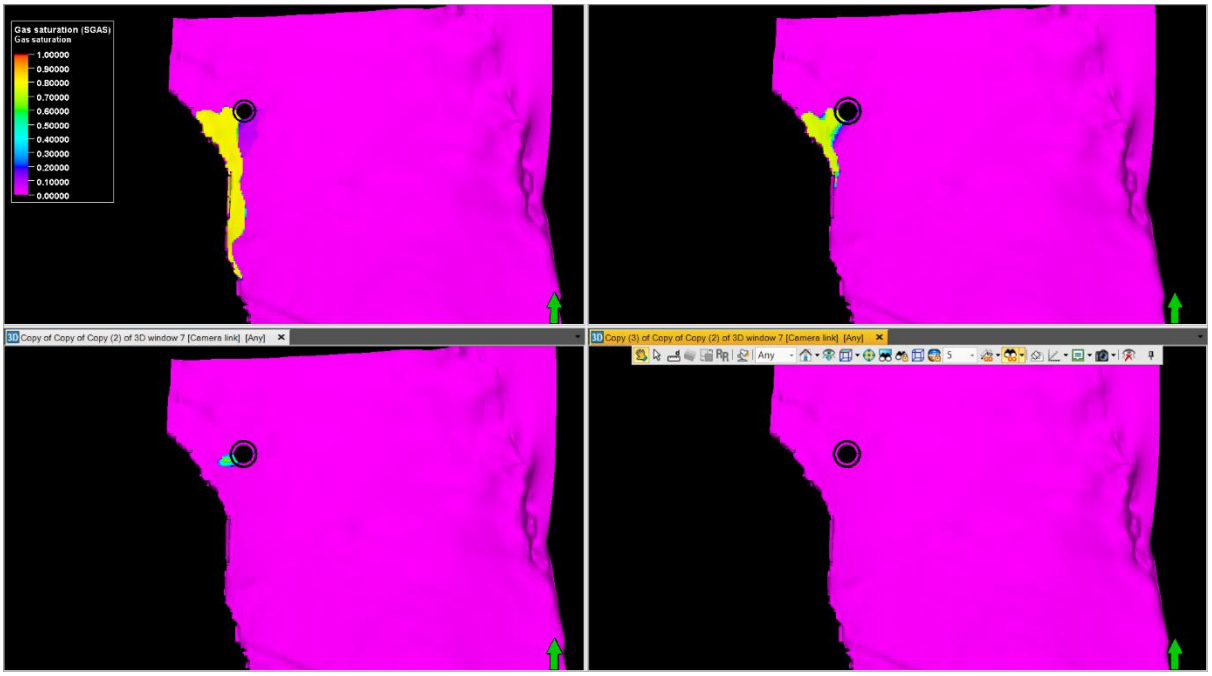

Figure 24 CO_2 plume distribution in 2072 for 100m grid size model. Linear Relperm : Upper Left. Relperm1: Upper right. Relperm2: Lower Left. Relperm3: Lower Right.

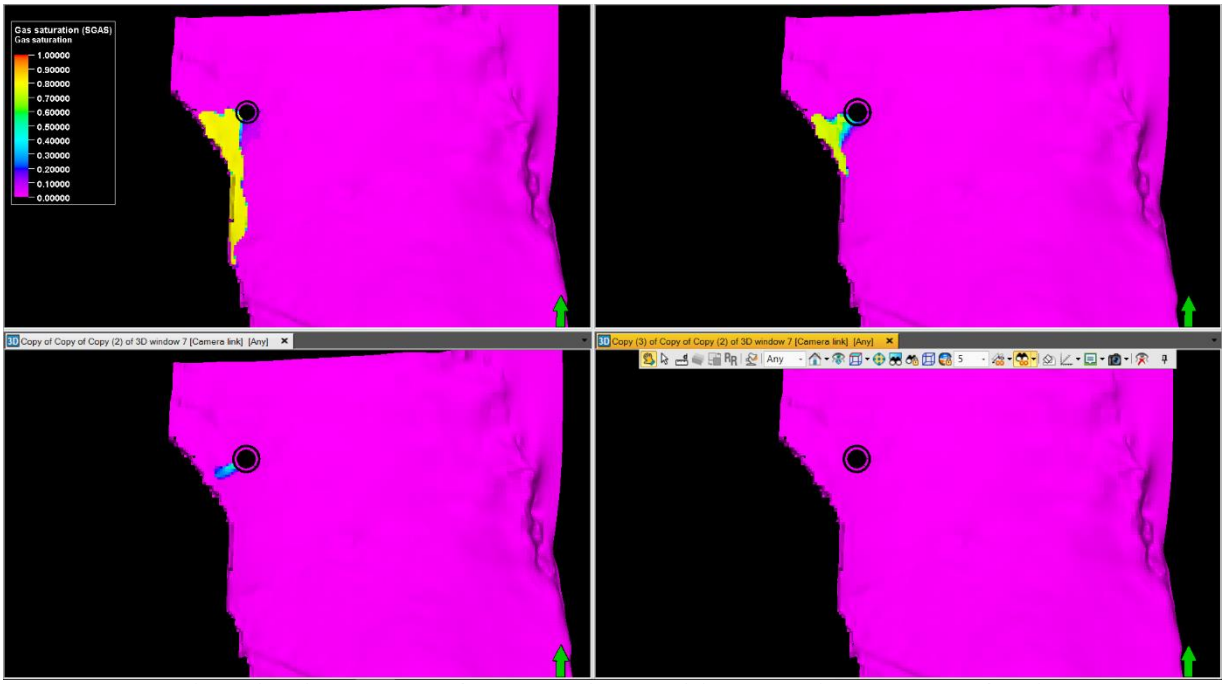

Figure 25 CO_2 plume distribution in 2072 for 150m grid size model. Linear Relperm: Upper Left. Relperm1: Upper right. Relperm2: Lower Left. Relperm3: Lower Right.

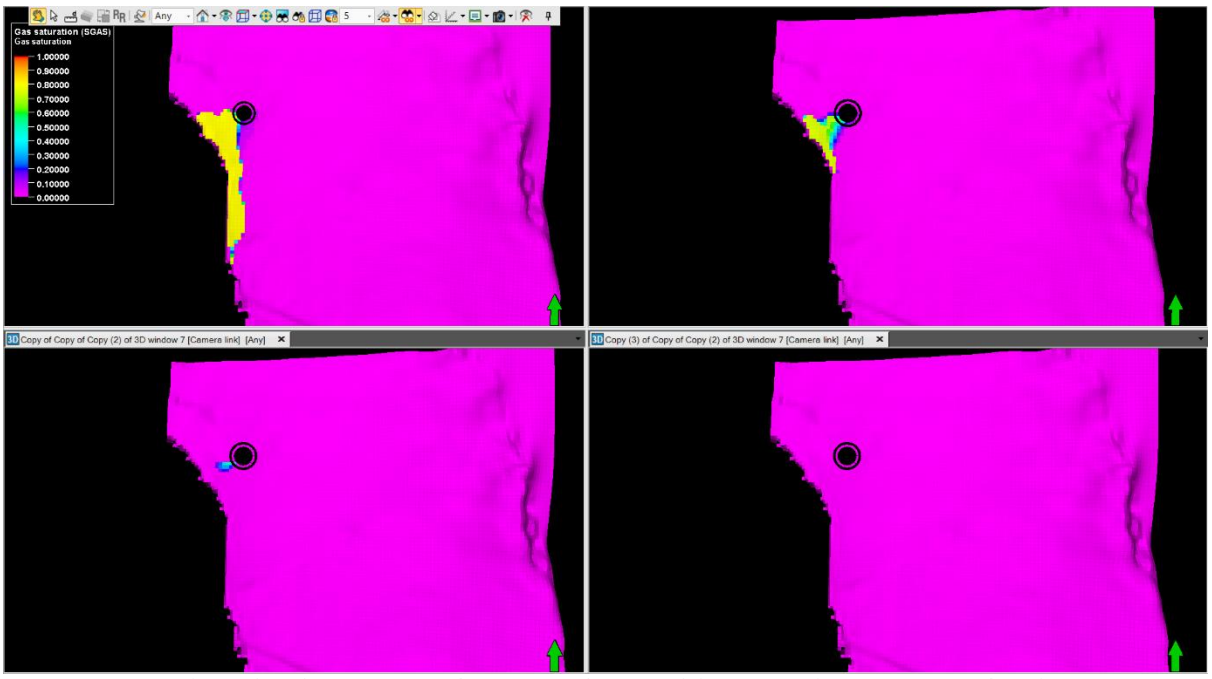

Figure 26 CO_2 plume distribution in 2072 for 200m grid size model. Linear Relperm : Upper Left. Relperm1: Upper right. Relperm2: Lower Left. Relperm3: Lower Right.

The results of the analysis reveal some interesting insights about how the grid size and relative permeability of the Alpha structure in the Smeaheia storage area impact the flow path of the CO_2 plume. The images in the upper left corner indicate that using linear relative permeability curves leads to the greatest spread of the CO_2 plume (Figures 24-26). Additionally, when using smaller grid sizes, the plume's spatial distribution shows an increased spread towards the southern portion of the Alpha structure (Figure 24). However, this effect is small and almost negligible.

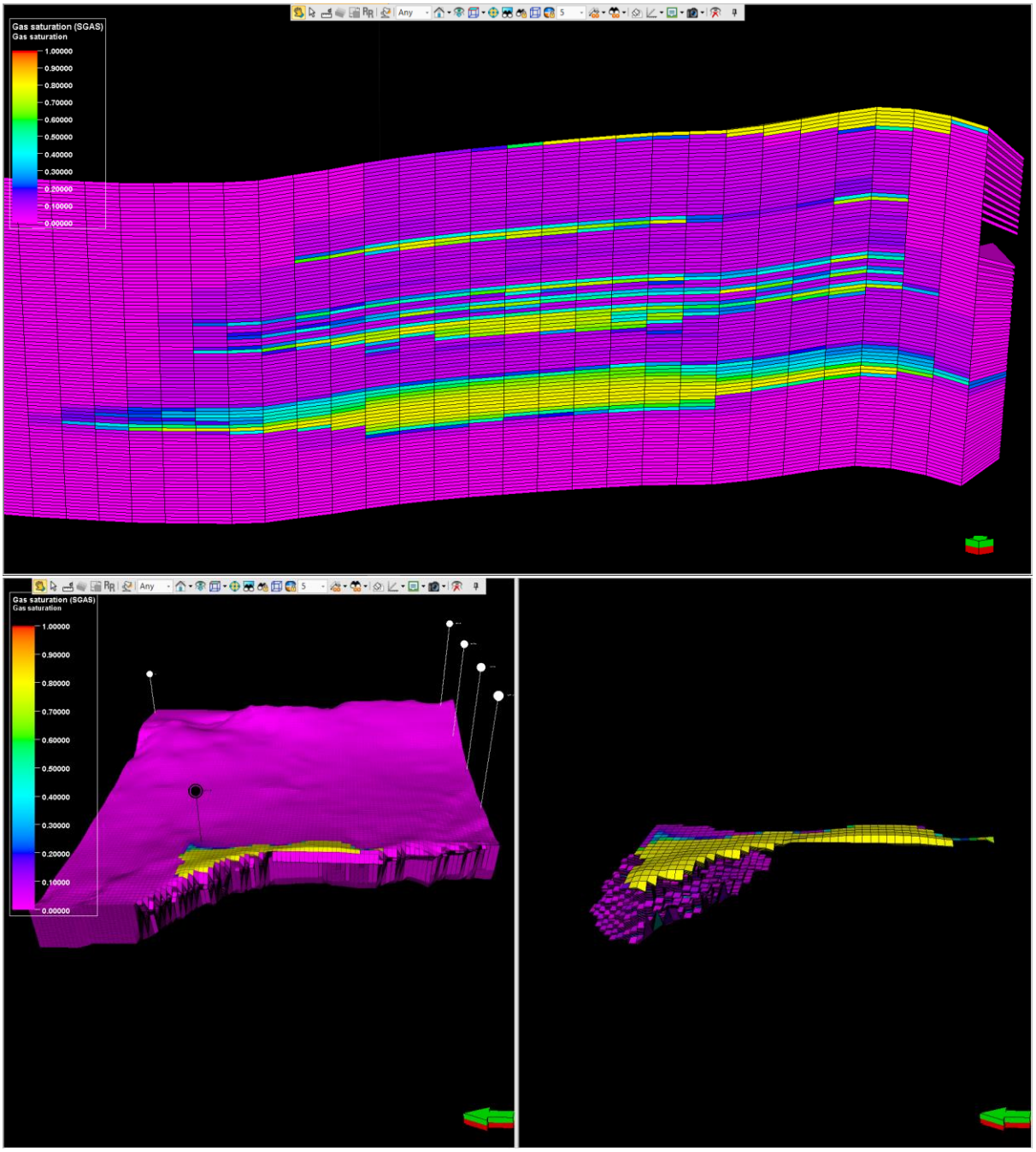

Figure 27 CO_2 Distribution for 200m grid model using Linear relative permeability. The lower right picture shows plume shape with gas saturations from 0.001 to maximum. The upper picture shows a side view of the reservoir with plume distribution in layers.

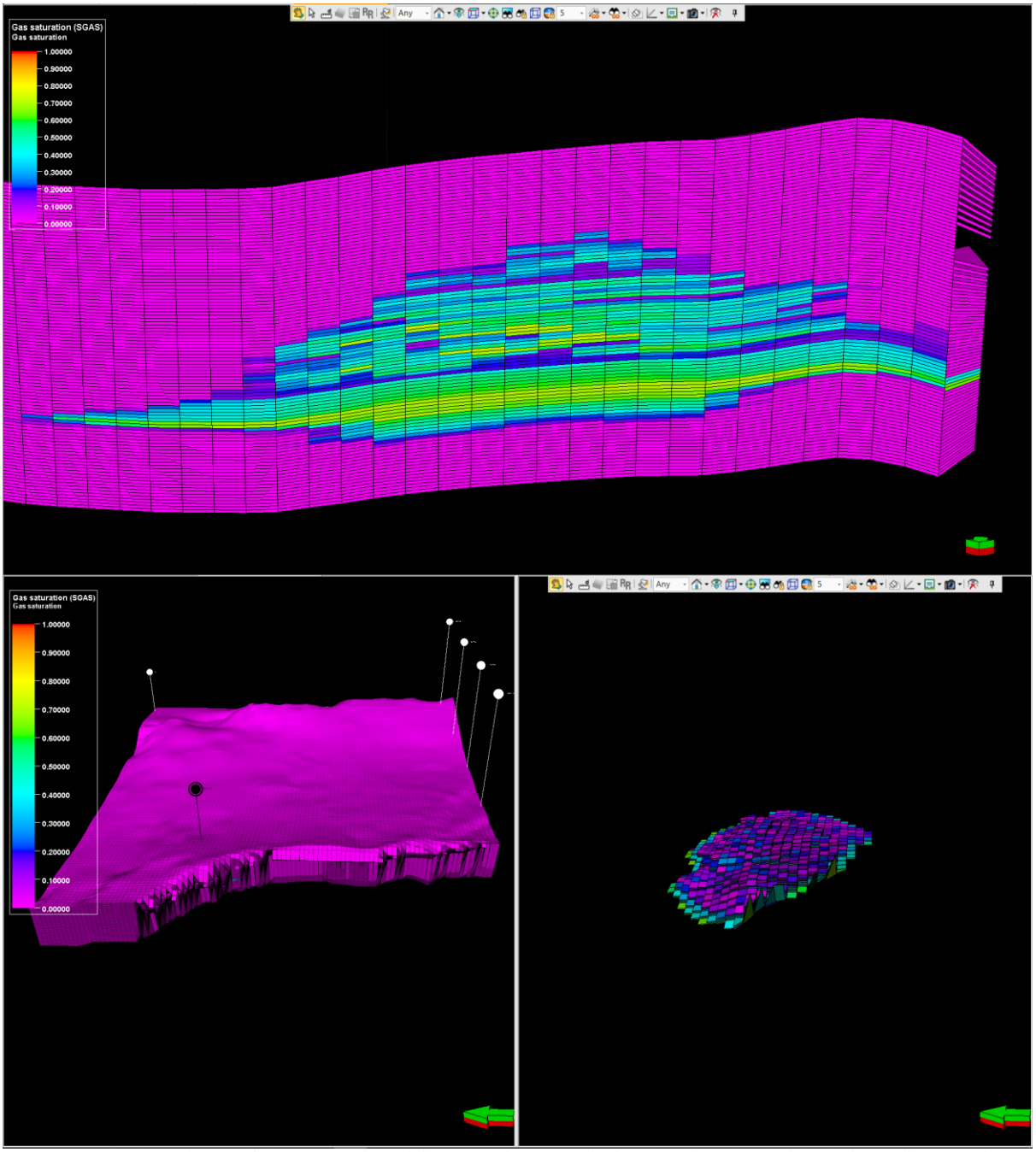

Figure 28 CO_2 Distribution for 200m grid model using Relperm3. The lower right picture shows plume shape with gas saturations from 0.001 to maximum. The upper picture shows a side view of the reservoir with plume distribution in layers.

Upon examining the images situated in the lower right-hand corner, which depict the distribution of the CO_2 plume through the implementation of the relperm3 relative permeability curve, it becomes quite evident that the plume has not propagated significantly towards the surface. Instead, most of its expansion is concentrated in the depper layers of the Alpha structure (Fig 28). This indicates that the CO_2 plume tends to move and spread predominantly in the lower regions of the reservoir, implying that there is a certain level of regulation and minimal movement in an upward direction. The utilization of the Relperm3 model reveals that CO2 exhibits reduced relative permeability when compared to the linear relative permeability curve. This diminished permeability hinders the mobility of the CO2 plume, resulting in slower movement and confinement

within the injection area. A visual examination of Figure 27 illustrates that the implementation of the linear relative permeability allows the plume to disperse more readily and explore additional vertical pathways under the influence of capillary forces.

The findings from this study offer valuable information about how the CO_2 plume behaves and interacts with the Alpha structure. It is crucial to accurately determine the relative permeability curves to effectively store and contain CO_2, as it plays a significant role in the plume's expansion. Furthermore, the size of the grid used affects how the plume is distributed spatially as seen in figures 24-26, highlighting the need to select an appropriate grid resolution to capture the complexities of CO_2 movement within the reservoir.

The research conducted has significantly contributed to our understanding of CO_2 plume dynamics by examining 3dimentional figures like figures 27 and 28. The findings provide crucial insights into how we can enhance dynamic reservoir simulation of CO_2 injection projects and develop effective storage systems in reservoir environments that are like the one in Smeaheia. Through a close examination of various factors such as pressure profiles, fluid saturations, and storage capacity estimations, we can better assess the feasibility and practicality of CO_2 storage in this field.

4.2. Field Pressure

To gain a better understanding of CO_2 storage reservoirs, it is essential to closely analyse the field pressure to analyse the field pressure results closely re results. These results provide valuable insights into how pressure changes during the injection and storage of CO_2. Accurate analysis and interpretation of this data are critical for evaluating the efficiency and effectiveness of CO_2 storage and assessing the storage site's long-term stability and integrity operations, as well as assessing the long-term stability and integrity of the storage site. In this section, we will focus on the key observations, trends, and implications for CO_2 storage operations based on the field pressure results obtained from the Smeaheia storage area.

Field pressure results are analysed for several reasons. Firstly, it is crucial to evaluate the pressure build-up and containment in the reservoir to maintain the site's integrity and avoid any potential CO_2 leakage. Additionally, we need to study the impact of grid size and relative permeability curves on pressure evolution to optimize injection parameters. This optimization will help us achieve efficient storage and desired pressure conditions.

When analysing field pressure data, it is crucial to recognize the uncertainties and limitations that may affect the accuracy of the results. These uncertainties may include the impact of production from the Troll field, fault transmissibility, and the effects of reservoir heterogeneity on pressure distribution.

The production from the Troll field and injection rate significantly impacts the Smeaheia field pressure. Five production wells in the model represent the production from the Troll reservoir.

Troll's gas production rate in March 2018 was estimated to be around 3.5 billion sm3 (Norwegian petroleum directorate, 2018). Studying this production is essential since it will impact the field pressure and CO_2 storage in Smeaheia.

The Smeaheia field and the Troll reservoir will have a pressure connection because of bridging faults and other geological connections. Given that the production rates in Troll are higher than the injection rates at Smeaheia, this connection will significantly impact how the pressure develops there. It can be seen from figures 29-31 that there is a 40-bar pressure drop before the start of the injection due to production from 5 wells which mimics production from the Troll field. The injected volume for all cases is 9000 tonnes per day and 81.125 Mt after 25 years of injection.

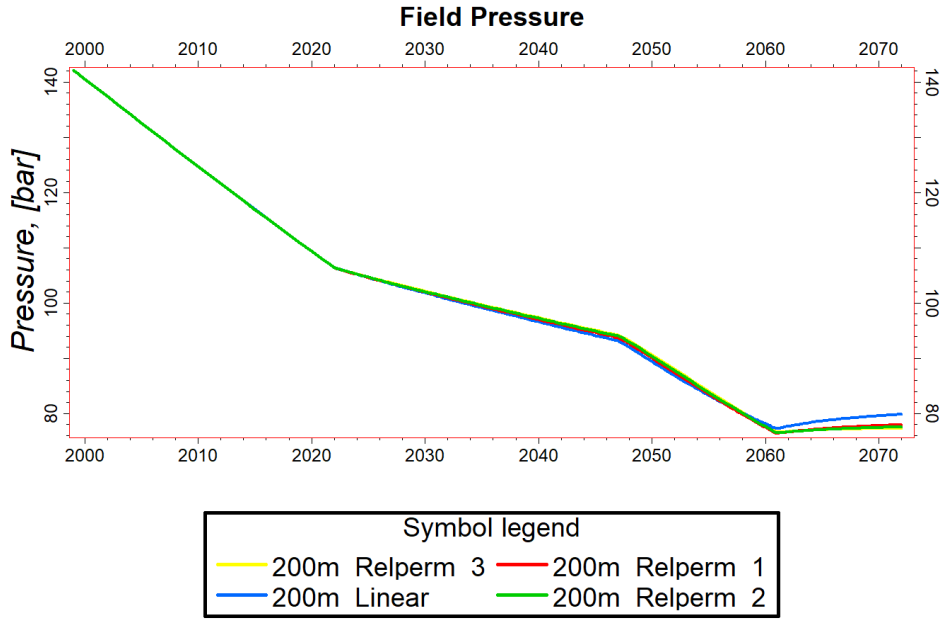

Figure 29 Field pressure trend for 200m grid size with different relative permeability curves.

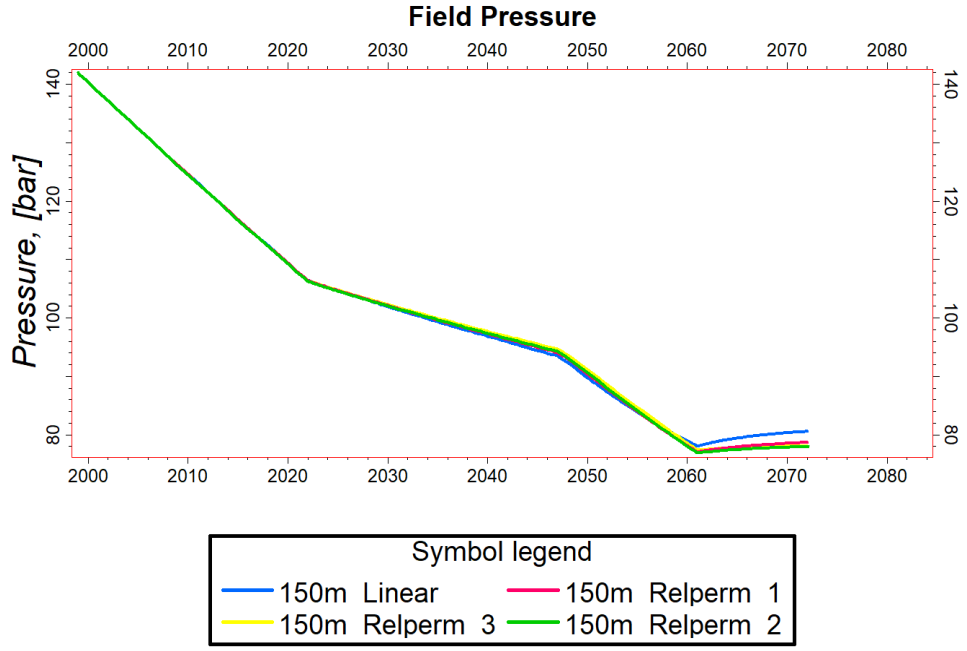

Figure 30 Field pressure trend for 150m grid size with different relative permeability curves.

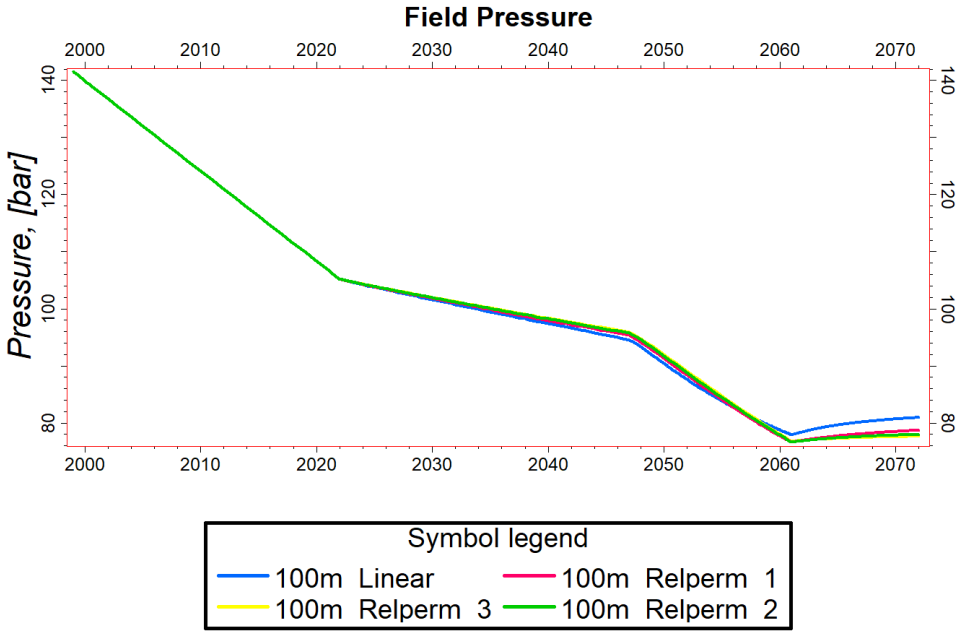

Figure 31 Field pressure trend for 100m grid size with different relative permeability curves.

Figures 29-31 show field pressure trend for different grid sizes. As it is obvious from the figures, cases with different relative permeability curves almost follow the same trend from the beginning of the simulation until start of injection in 2022, since the only present phase in the system is water and relative permeability concept does not exist with only one phase, then the end of injection in 2047 and the end of production in 2060. But it can be seen that after 2060 there is a sharp increase in field pressure for cases using linear relative permeability. As it was shown in chapter 3, field pressure follows the same trend for different grid sizes utilizing the same relative permeability.

In 2060, a noticeable pressure behavior can be observed when the production wells are closed. Specifically, in the scenario where a linear relative permeability curve is present, there is a sharp increase in the field pressure compared to the other cases. This occurrence is due to the CO_2 migrating towards shallower layers of the reservoir, where the pressure is relatively lower. As a result, the pressure behavior becomes distinguishable and noteworthy.

CO_2 can move more easily towards shallower regions with lower pressure due to buoyancy forces and its enhanced mobility, which is enabled by a linear relative permeability curve. The fluid flow behavior in porous media is governed by relative permeability properties, resulting in the preferential movement of CO_2 towards shallower depths. This movement causes the CO_2 to expand, contributing to the observed increase in field pressure. As CO_2 displaces other fluids in the reservoir and occupies more space, the overall pressure rises. However, CO_2 expansion in shallower depths can lead to containment problems, as gaseous CO_2 is more prone to leakage.

These findings emphasize the importance of accurately characterizing relative permeability properties in reservoir simulations. Precise calibration and validation based on experimental data or field measurements are crucial for improving the accuracy and reliability of simulations, allowing for better predictions of pressure evolution and CO_2 distribution. The observed pressure dynamics and CO_2 expansion highlight the potential for larger storage capacities in deeper regions, but careful monitoring and management of higher pressures are necessary to ensure the long-term integrity and stability of CO_2 storage operations.

4.3. Bottomhole pressure

Examining bottomhole pressure data is a critical component in assessing the effectiveness of CO_2 injection and storage operations within subsurface reservoirs. This type of data provides valuable insights into pressure behavior at the injection wellbore, allowing for the evaluation of injection rates, pressure containment, and overall reservoir response. Within this section, we will go into detail about the bottomhole pressure results obtained from the CO_2 injection well located in the Smeaheia storage area. Our focus will be on identifying crucial observations, trends, and their implications for the success of the CO_2 storage project.

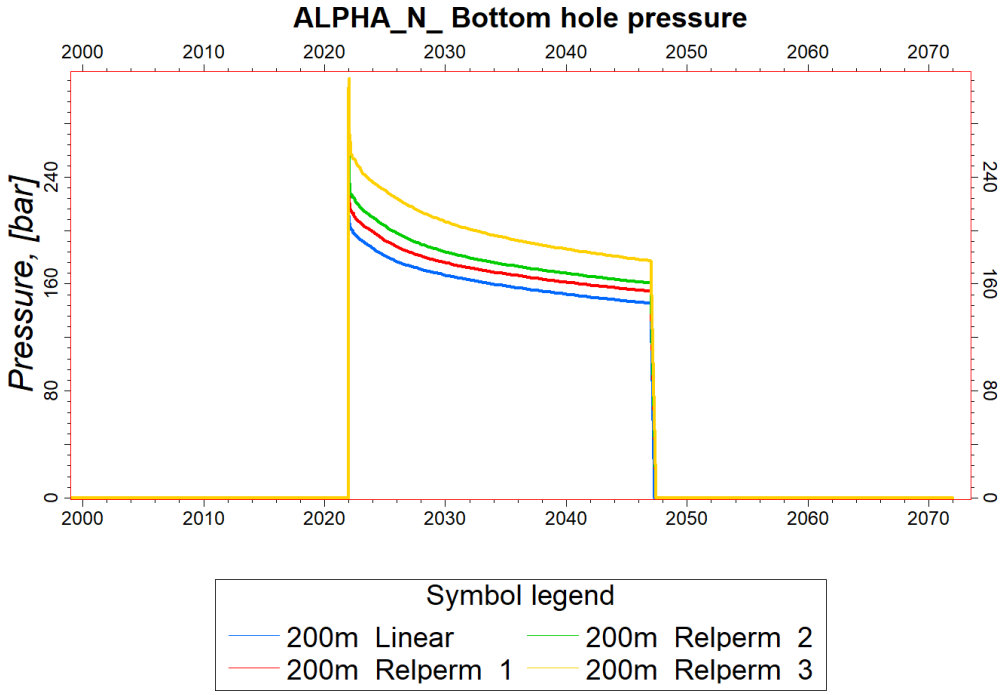

Figure 32 Bottom-hole pressure of 200m grid size cases with different relative permeability curves.

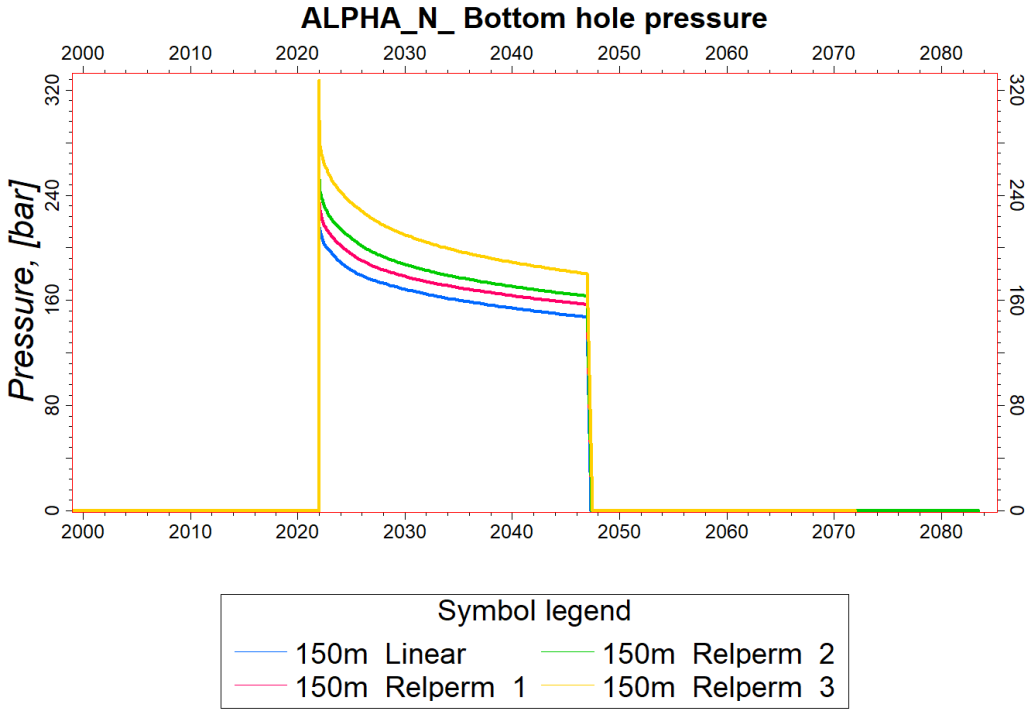

Figure 33 Bottom-hole pressure of 150m grid size cases with different relative permeability curves.

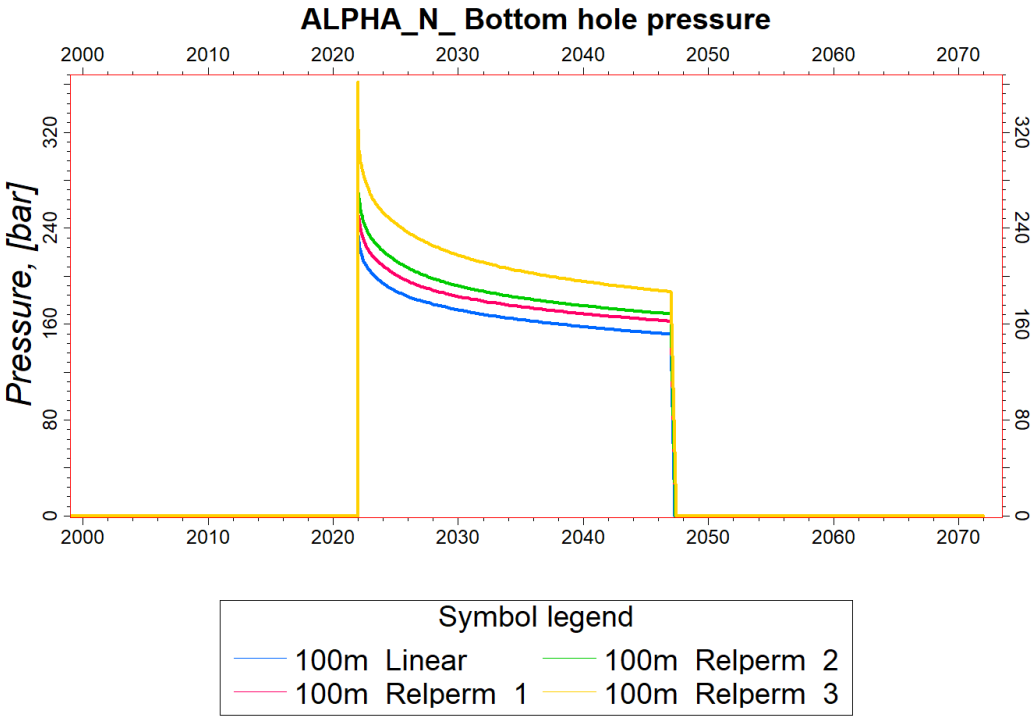

Figure 34 Bottom-hole pressure of 100m grid size cases with different relative permeability curves.

Figures 32-34 showcases four distinct relative permeability curves and bottom-hole pressure profiles for injection well Alpha-N. These profiles were established using grid sizes of 100, 150, and 200 meters. It is crucial to point out that the figures illustrate that the "relperm3" relative permeability model yields the highest bottom-hole pressures. This model recorded a maximum pressure of 360 bar during the initial injection stages. The reason for this observation can be attributed to the unique characteristics of the "relperm3" relative permeability curve. In this particular model, the relative permeabilities of both the injected CO_2 and brine are comparatively low. As a result, when CO_2 is injected into the formation, it faces more significant challenges in displacing the formation fluids due to the lower permeability and saturation level of CO_2. This increased resistance to fluid flow leads to a higher bottom-hole pressure being recorded during the early stages of injection, which is distinguished by a clear peak.

On the other hand, the scenarios that utilize a linear relative permeability curve display the most favorable outcomes in terms of bottom-hole pressure. This result can be attributed to the relatively higher relative permeabilities observed during the initial injection phase. These increased relative permeabilities enable a smoother displacement of brine by CO_2, resulting in less resistance and ultimately leading to lower bottom-hole pressures.
Relative permeability properties have a critical influence on bottom-hole pressure profiles. The characteristics of the relative permeability curves affect flow behavior and fluid displacement during injection operations. Lower relative permeabilities of CO_2 and brine make moving CO_2 through the formation more challenging, resulting in higher bottom-hole pressures. The linear relative permeability curve allows for more efficient brine displacement by CO_2, resulting in lower bottom-hole pressures. Proper characterization and selection of relative permeability models are crucial for accurate predictions of bottom-hole pressures and fluid flow dynamics in CO_2 injection operations. This contributes to a better understanding of injection processes and optimal outcomes.

In Figure 35, we can see the bottom-hole pressure profiles of well Alpha-N. The focus is on grid sizes of 100, 150, and 200 meters while using the linear relative permeability curve. By analyzing the figure, we can observe a clear pattern. The 100-meter grid size shows a significant increase of 20 bars in bottom-hole pressure at the beginning of the simulation. The difference in bottom-hole pressure trends is due to the more precise 100-meter grid size. The higher-resolution grid captures and includes these variations in closer proximity to the well, thus resulting in a stronger pressure response. When CO_2 is injected into the reservoir, it interacts with the fluid and rock properties, leading to fluid flow and pressure changes. The finer grid resolution introduces more grid blocks, which increases the total flow path and flow resistance within the reservoir. The finer grid resolution enables a more detailed representation of the reservoir's heterogeneities, resulting in amplified pressure response and increased flow resistance.

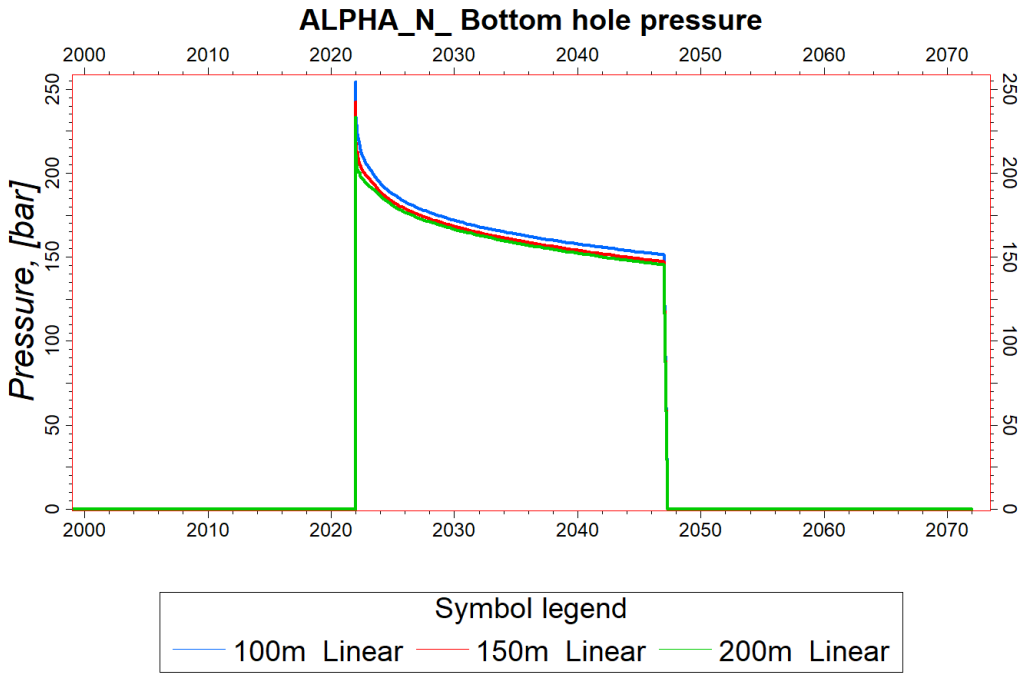

Figure 35 Bottom-hole pressure of cases with grid sizes 100, 150 and 200 meters utilizing linear relative permeability.

It is crucial to select the right grid size when simulating fluid flow behaviour and predicting pressure distribution near the wellbore. The grid size should capture essential reservoir features while maintaining computational efficiency. The observed variations in bottom-hole pressure trends based on grid sizes provide insight into reservoir dynamics and can help with decision-making and optimization processes.

4.4. Simulation run-time

The simulation run-time report is an important document that provides a detailed analysis of the performance and efficiency of a reservoir simulation model. It shows how long it took to complete various simulation scenarios and highlights any significant differences in the time it took for each case. By carefully examining this data, we can assess the resources used, identify any potential problems, and evaluate how well the simulation process is working. This report is essential for decision-makers who want to make sure the simulation process is as efficient as possible.

The purpose of the report is to find differences in the time it takes to run different simulation cases. These differences can happen because of changes in the input parameters, model complexity, or computational settings. By analyzing these differences, we can identify areas where optimization is needed or where more computational resources are necessary. Table 8 shows the configuration of the system used for running simulations.

System type	*Personal Laptop*
CPU model	Ryzen 9 5900 HS
CPU cores	8 (16 logical)
CPU base speed	3.3 GHz
Memory	16 GB
Memory speed	4266 MHz

Table 6 System configuration.

Run-time [Hours]	*Linear relperm*	*Relperm1*	*Relperm2*	*Relperm3*
100m	19.5	9	6.5	5.3
150m	8	7	5	3
200m	0.65	1.5	1.16	1

Table 7 Run-time hours for simulation cases.

Reservoir simulations' computational run-time depends on various factors, such as the model's size, fluid flow dynamics, reservoir heterogeneities, and numerical models used. However, this study mainly concentrates on examining how simulation run-time is affected by relative permeability and grid size. Each case's simulation run-time data is available in Table 9, taken from RTELOG of each simulation.

Based on Table 9, it is evident that the relative permeability significantly impacts the simulation run-time for grid sizes of 100m and 150m. Specifically, the linear permeability model requires the most time to execute due to the increased computational effort that is necessary for mass balance calculations. This is because both CO_2 and brine possess higher relative permeability values, which results in a more extensive mass transfer between grid blocks that must be calculated for each time step. It is important to note, however, that this conclusion cannot be generalized to the scenario with a grid size of 200m.
According to the analysis presented in Table 8, it is evident that the size of the grid plays a

crucial role in determining the simulation run-time. When the grid resolution is finer, the simulation takes a longer time to run as the simulator has to calculate for each grid block at every time step. As the number of grid blocks increases, the simulation run-time also increases proportionally since more computational power is required to simulate the entire model.

It is worth mentioning that, in this study, we reduced the size of the model to improve computational efficiency and run-time. This approach aims to capture the essential features of the reservoir system while exploring the influence of relative permeability and grid size on simulation run-time. The reduction in model size does not compromise the overall accuracy and validity of the findings.

5. Conclusion

In the conclusion section of this thesis, a detailed summary and analysis of the research conducted on the movement of CO_2 plume and its impact on grid size and relative permeability in carbon capture and storage (CCS) projects are presented. The section aims to consolidate the study's objectives, emphasize the importance of the research outcomes, and provide actionable recommendations for the progression of CCS initiatives.

The study reveals that the relative permeability curve significantly affects various parameters, including pressure changes, CO_2 movement, and simulation run-time. Relative permeability affects pressure dynamics, storage capacity, and the overall efficiency of CO_2 injection and storage operations. Identifying and calibrating relative permeability characteristics is crucial for CCS project managers and stakeholders. To ensure accurate reservoir simulations, it's important to well-characterize relative permeability values through experimental data or field measurements. This leads to better forecasts for CO_2 movement, pressure evolution, and storage capacity, which improves project planning, risk assessment, and operational decision-making.

When simulating CO_2 storage projects, it is important to use accurate grid sizes to achieve reliable and precise results. Finer grids can better represent the complex properties of the reservoir, resulting in more accurate depictions of fluid flow behavior and CO_2 plume migration. However, it is important to remember that using small grid sizes means more computing work and longer simulation times, which can affect project schedules and resource allocation. Therefore, it is crucial to find the right grid size that balances the need to capture important features and heterogeneities with computational efficiency. Accurate upscaling techniques must be employed to determine the optimal grid size that ensures reliable and efficient reservoir simulation. By carefully weighing these factors, project managers can select a grid size that best suits their needs.

The investigation shows that CO_2 storage in the Smeaheia field's Alpha structure is promising, with a capacity estimated to be over 80 million tonnes. During the 50-year monitoring period, 81.125 million tonnes of CO_2 were efficiently injected into the Alpha structure without any movement towards the Beta structure or spill point. This result confirms the Alpha structure's capability to contain the injected CO_2 within the defined storage zone. However, the economic aspects have not been discussed in this study and feasibility of CO_2 Storage in Smeaheia can not be concluded here.

It is important to consider the potential for CO_2 leakage from both the Alpha and Beta structures. The Beta structure is at a higher risk due to its shallower depth, which could cause the CO_2 to turn into a gas, and uncertainties regarding Øygarden fault. However, we also need to assess the risk of leakage from the Alpha structure and take necessary precautions to ensure it remains secure during the storage process. This involves regularly assessing the Alpha structure's structural integrity, monitoring pressure and CO_2 movement, and implementing measures to minimize the risk of leakage.

6. Recommendation for Further Research

In order to enhance the reliability and precision of reservoir simulations in the Smeaheia field, it is crucial to gather experimental data on relative permeability and fluid dynamics in the Smeaheia field. Additionally, exploring the effect of CO_2 solubility in brine can offer valuable insights into the behavior of CO_2 plumes during storage operations. To ensure that the simulations are accurate and efficient, it is recommended to rebuild the static model with finer grids and employ suitable upscaling techniques to accurately capture the heterogeneities and characteristics of the reservoir.

7. Bibliography

(IEA), I. E. A., u.d. [Internett]
Available at: https://www.iea.org/

Ajayi, T., 2019. A review of CO2 storage in geological formations emphasizing modeling, monitoring and capacity estimation approaches. *Petroleum Science.*

Al-Hinai, K., Al-Bemani, A. and Vakili-Nezhaad, G., 2014. Experimental and theoretical investigation of the CO2 minimum miscibility pressurefor the omani oils for CO2 Injection EOR method.. *nternational Journal of Environmental Science and Development.*

Amiri, B., 2022. *A Fast and Accurate Investigation into CO2 Storage Challenges by Making a Proxy Model on a Developed Static Model with The Application of Artificial Intelligence/Machine Learning,* s.l.: POLITECNICO DI TORINO.

Anderson, W., 1987. Wettability Literature Survey Part 5: The Effects of Wettability on Relative Permeability. *SPE.*

Anon., u.d. *Petrolblogweb.* [Internett]
Available at: https://petroblogweb.wordpress.com/

Anon., u.d. *Petrowiki.* [Internett]
Available at: https://petrowiki.spe.org/PetroWiki

Bachu, S., 2008. CO2 storage in geological media: Role, means, status and barriers to deployment. *Progress in Energy and Combustion Science.*

Bachu, S., 2015. *Review of CO2 storage efficiency in deep saline aquifers.* s.l., s.n.

Baroudi, H., 2021. A review of large-scale CO2 shipping and marine emissions management for. *Applied Energy,* p. 42.

Batycky, R.P and Thiele, M.R., 2007. Reservoir Simulation. I: *Petroleum Engineering Handbook vol.6.* s.l.:Society of Petroleum Engineers.

Benson, S.M. and Cole D.R, 2008. CO2 Sequestration in Deep Sedimentary Formations. *Elements.*

Benson, S. et al., 2005. *Underground geological storage,* s.l.: IPCC special report on carbon.

Brobakken, I. I., 2018. *Modeling of CO2 Storage in the Smeaheia,* Trondheim: NTNU.

Bruce, H., Hovorka, S. and Melzer, S., 2012. Geologic carbon storage through enhanced oil recovery.. *Energy Procedia 37.*

Burton, M., Kumar, N. and Bryant S.L., 2009. CO2 injectivity into brine aquifers: Why relative permeability matters as much as absolute permeability. *Energy Procedia.*

CO2Datashare, u.d. *CO2Datashare.* [Internett]
Available at: https://co2datashare.org/dataset/smeaheia-dataset

Cooper, C., 2009. A technical basis for carbon dioxide storage. *Energy Procedia.*

Corey, A. & Brooks, R., 1964. Hydraulic Properties of Porous Media. I: s.l.:Colerado State University.

Doughty, C. and Pruess, K., 2004. Modeling supercritical carbon dioxide injection in heterogeneous porous media. *Vadose Zone J., 3, 837– 847.*

Dreyer, T., Whitaker, M., Dexter, J., Flesche, H. and Larsen, E., 2005. *From spit system to tide-dominated delta: integrated reservoir model of the Upper Jurassic Sognefjord Formation on the Troll West Field.*. London, s.n.

Eide, L., 2019. *Enabling Large-Scale Carbon Capture, Utilisation, and Storage (CCUS) Using Offshore Carbod Dioxide (CO2) Infrastructure Developments—A Review,* s.l.: Energies.

Elenius, M. and Kaufmann R., 2018. Assessment of CO2 storage capacity based on sparse data: Skade Formation. *International Journal of Greenhouse Gas Control.*

European_Commission, 2018. *A Clean Planet for all - A European strategic long-term vision for a prosperous, modern, competitive and climate neutral economy,* s.l.: s.n.

Flett, M., Gurton, R. and Taggart, I., 2004. *The function of gas-water relative permeability hysteresis in the sequestration of carbon dioxide in saline formations.* Perth, Australia, s.n.

Furre, A., 2019. Building confidence in CCS: From Sleipner to the Northern Lights Project. *First Break.*

Gibbins, J., 2008. Carbon capture and storage. *Energy Policy.*

Global CCS, I., u.d. *Global CCS Institute.* [Internett]
Available at: https://www.globalccsinstitute.com/about/what-is-ccs/
[Funnet 16 12 2022].

Goldsmith, P., 2000. Exploration potential east of the Troll Field, offshore Norway, after dry well 32/4-1. *Norwegian Petroleum Society Special Publications.*

Grude, S., Landrø, M. and Dvorkin, J., 2014. Pressure effects caused by CO2 injection in the Tubåen Fm., the Snøhvit field.. *International Journal of Greenhouse Gas Control 27.*

Hansen, J., 2005. Efficacy of climate forcings.. *ournal of geophysical research: atmospheres 110.D18.*

Hill, B., 2013. Geologic Carbon Storage Through Enhanced Oil Recovery. *Energy Procedia.*

Hoff, K. A., 2017. *CO2 capture - Absorption Processes.* [Internett]
Available at: https://www.sintef.no/en/expertise/sintef-industry/process-technology/co2-capture-absorption-processes/
[Funnet 16 12 2021].

Holgate, N., 2013. Sedimentology and sequence stratigraphy of the Middle–Upper Jurassic Krossfjord and Fensfjord formations, Troll Field, northern North Sea. *Petroleum Geoscience.*

IPCC, 2014. *Climate Change 2014: Synthesis Report. Contribution of Working Groups I, II and III to the Fifth Assessment Report of the Intergovernmental Panel on Climate Change [Core Writing Team, R.K. Pachauri and L.A. Meyer (eds.)].,* Geneva, Switzerland: IPCC.

Kopp, A. C. H. a. H. R., 2009. Investigations on CO2 storage capacity in saline aquifers Part 1. Dimensional analysis of flow processes and reservoir characteristics. *Int. J. Greenhouse Gas Control.*

Kumar, A., Ozah, R., Noh, M., Pope, G.A., Bryant, S., Sepehrnoori, K. and Lake, L.W., 2005. Reservoir Simulation of CO2 Storage in Deep Saline Aquifers. *SPE.*

Lauritsen, H., 2018. Assessing Potential Influence Of Nearby Hydrocarbon Production On CO2 Storage At Smeaheia. *European Association of Geoscientists & Engineers.*

Li, Z., Fernandes, P. and Zhu, D., 2011. Understanding the Roles of Inflow-Control Devices in Optimizing Horizontal-Well Performance. *OnePetro.*

Lothe, A.E., Bergmo, P., Emmel, B.U. and Eliasson, P., 2018. Effects of uncertainties in fault interpretations on pressure depletion and CO2 storage injection at Horda Platform, offshore Norway. *14th International Conference on Greenhouse Gas Control Technologies, GHGT-14 21st -25th October 2018, Melbourne, Australia.*

Lothe, A.E., Grimstad, A. and Bergmo, P.E., 2019. Storage Resources for Future European CCS Deployment; A Roadmap for a Horda CO2 Storage Hub, Offshore Norway. *SINTEF Academic Press.*

Madani, S., 2023. *Reservoir Modeling of CO2 Storage in the Smeaheia Field (Specialization project report),* Trondheim: NTNU.

Mateus, A., 2007. *Analysis of radiation properties of gases and utilization,* s.l.: The University of Lisbon.

Metz, B., 2005. Intergovernmental panel on climate change special report on carbon dioxide capture and storage. *Cambridge, UK and New York, USA.*

Miri, R., 2015. New insights on the physics of salt precipitation during injection of CO2 into saline aquifers.. *International Journal of Greenhouse Gas Control 43.*

Mulrooney, M., 2020. Structural analysis of the Smeaheia fault block, a potential CO2 storage site,. *Marine and Petroleum Geology,* p. 33.

Nazarian, B., 2021. *Reservoir engineering of CO2 storage (NTNU Presentation),* Trondheim: s.n.

Nord, L. & Bolland, O., 2020. *Carbon Dioxide Emission Managemenet in Power Generation.* s.l.:Wiley.

Pawar, R., 2015. Recent advances in risk assessment and risk management of geologic CO2 storage. *International Journal of Greenhouse Gas Control.*

Rahmana, M.J., Choib, J.C., Fawada, M. and Mondol, N.H, 2021. Probabilistic analysis of Vette fault stability in potential CO2 storage site Smeaheia, offshore Norway. *Elsevier.*

Ringrose, P., 2020. *How to Store CO2 Underground: Insights from early-mover CCS Projects.* s.l.:Springer.

Ringrose, P., 2021. *CO2 Storage: Operation and Integrity of Engineered CO2 Storage (4. Thermodynamics and Transport),* Trondheim: s.n.

Rutqvist, J., 2012. The Geomechanics of CO2 Storage in Deep Sedimentary Formations. *Geotechnical and Geological Engineering.*

Skurtveit, E., Aker, E., Soldal, M. and Angeli, M. and Wang Z., 2012. Experimental investigation of CO2 breakthrough and flow mechanisms in shale. *Petroleum Geoscience.*

Statoil, 2016. *internal report on Subsurface Evaluation of Smeaheia,* s.l.: Statoil.

Wegener, D.C. and Harpole, K.J., 2010. *Determination of relative permeability and trapped gas saturation for predictions of WAG performance in the South Cowden CO2 flood.* Tulsa, Oklahoma., s.n.

Wildbolz, C., 2007. *Life cycle assessment of selected technologies for CO2 transport and sequestration.,* Zurich: Swiss Federal Institute of Technology.

Zhou, X., 2021. CO2 huff-n-puff process to enhance heavy oil recovery and CO2. *Elsevier.*

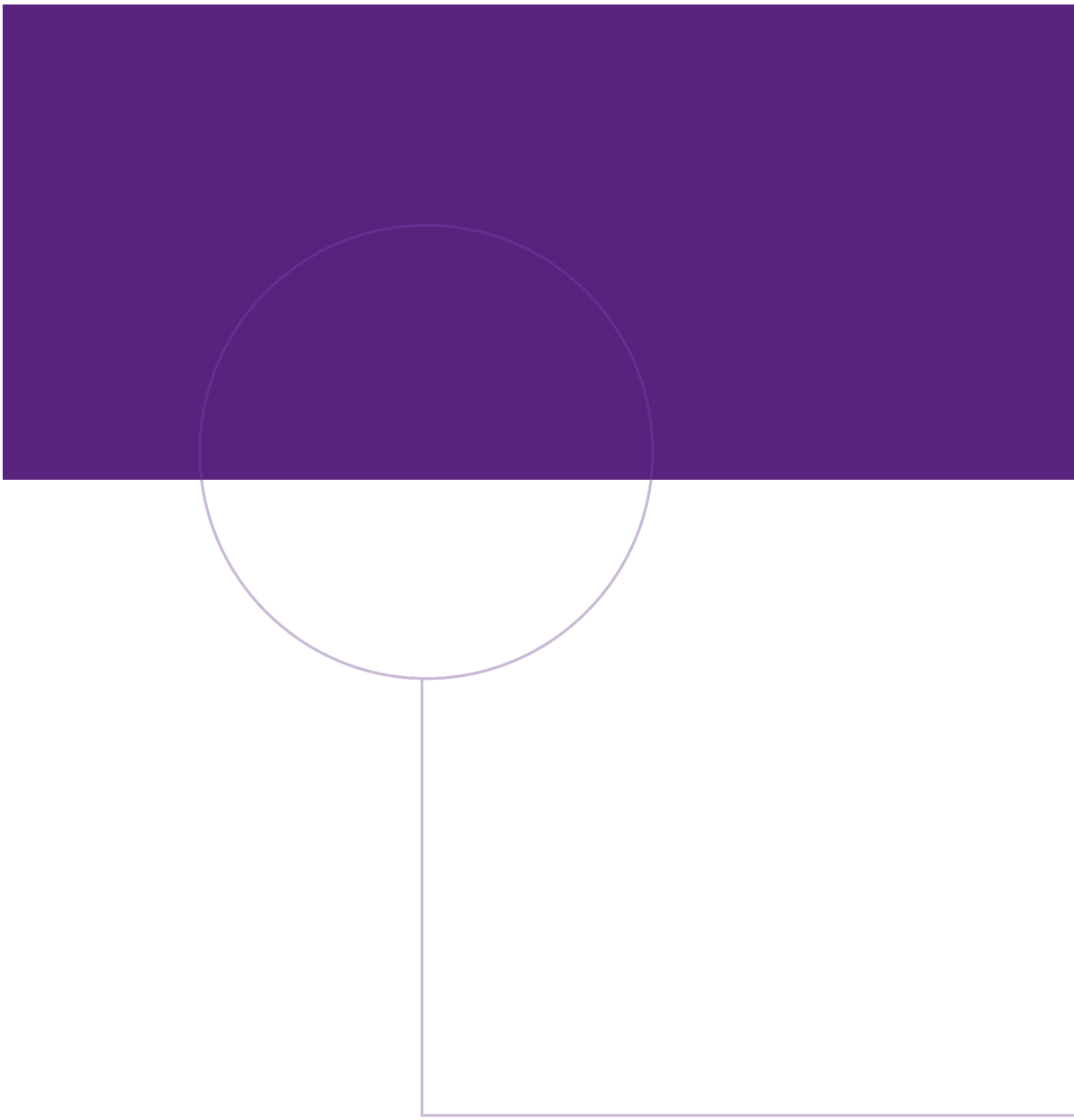

NTNU

Norwegian University of
Science and Technology